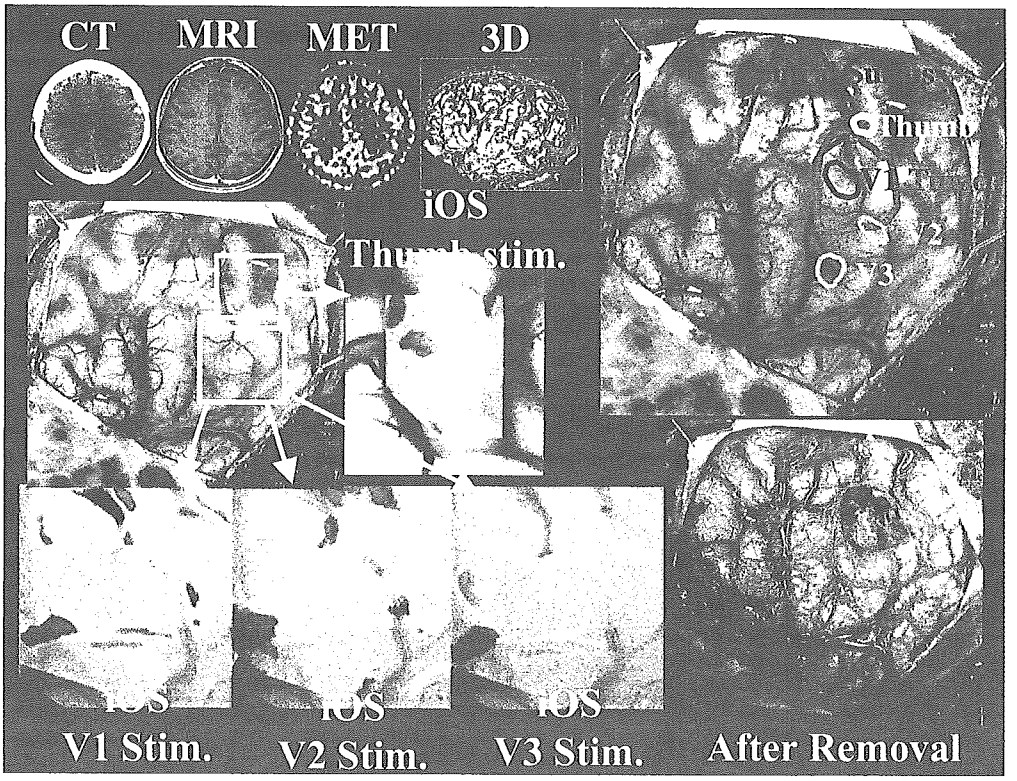

FIG. 4. Case 12. Images obtained in a patient with oligodendroglioma in the face sensory area in the left hemisphere. A small calcified spot without enhancement revealed high uptake of MET on PET scanning. Intrinsic optical signals (iOS) elicited by stimulation of the thumb and first, second, and third branches of the TN (V1, V2, and V3, respectively) are shown. The tumor area determined on MET-PET scanning was totally resected. The resected area included a portion of cortex with optical signals to the first and second branches of TN stimulation. The portion of cortex with the optical signals elicited on thumb stimulation was not injured. Transient weakness in the upper extremity and dysphasia occurred postoperatively, presumably due to postoperative edema, but these problems improved in 10 days.

have already developed a technique of imaging the neuronal circuits of hierarchically organized human primary sensory cortex.[33] All of these reports attest to the scientific usefulness of optical imaging for investigating the mechanisms of human cerebral/cortical/neuronal circuits.

In the present report, we analyzed how optical imaging of human brain function may be applied practically as an intraoperative monitoring method during brain tumor surgery. Somatosensory optical signals were detected on the primary sensory cortex in all patients in a state of anesthesia (inhaled) as were SSEPs. When comparing the characteristics of optical imaging with those of the ordinary evoked potential method, we noted that the former had several advantages. The optical signal obtained using our acquisition protocol has been reported to represent accurately the electrical neuronal activity together with a well-established physiological background.[22,32,33,39,44] On this basis, we can actually delineate functioning cortex against certain stimuli. This process provides spatial resolution superior to that supplied by electrophysiological recording with cortical electrodes, a method that enables one to draw a topographic map by using electrodes placed with 5- to 10-mm intergaps without visualizing the actually activated area. As demonstrated in our optical recording analysis, the cluster of cortical structures responding to a single sensory stimulus measures less than 10 mm in diameter. As such, recording with saucer electrodes may not be enough to locate the functioning area. Another disadvantage of cortical SSEP monitoring is that it depends not on the direct recording of an action potential, but on the phase reversal of the current dipole. In this condition, the natural bend of the central sulcus at the hand portion[30] or the deformation of the central sulcus by the tumor's mass effect may lead to misinterpretation of the results, as occurred in two cases in the present study (Fig. 1C and D). Moreover, phase reversal is not a reliable method of localizing the central sulcus of the face sensorimotor area.[21] Meanwhile, we demonstrated that the face sensory response could be clearly recorded by distinguishing its representations on the different trigeminal branches on the surface of the primary sensory cortex.[33,35] This detailed mapping of somatotopic representations of sensory responses successfully revealed the resection border for gliomas in the sensorimotor cortex in patients in the present study.

Although maximal resection while preserving brain function is crucial in glioma surgery, this principle is generally difficult to realize when the tumor is located in the eloquent gyrus. The sensorimotor cortex is a highly eloquent area, but partial resections of this area are an option when circumstances permit. Functional deficits from resections of the face motor cortex can be avoided if the border between face and hand motor areas is correctly determined and the hand area is secured.[8,17,18,25] In our view, resection of the sensory cortex may be permissible when it will not interfere with the functional living requirements of patients. For most

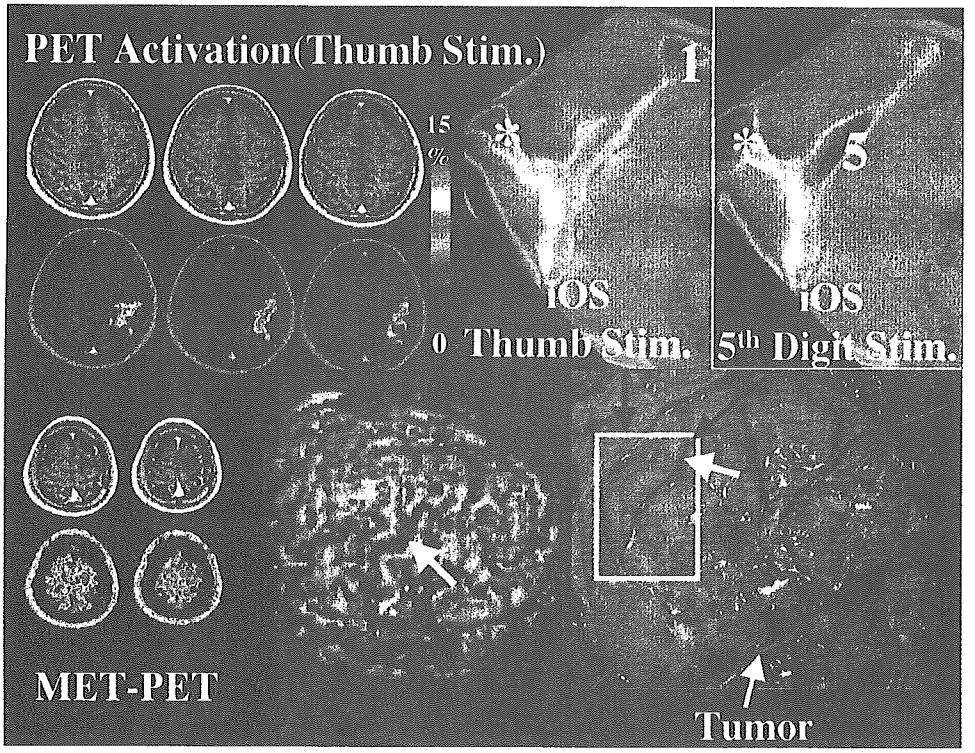

FIG. 5. Case 10. Images obtained for a comparison of PET sensory activation, intrinsic optical signal (iOS), and intraoperative findings in a patient with an oligodendroglioma in the left premotor area. The tumor area was delineated on MET-PET scanning. *Upper Left:* Results of a PET activation study with $H_2{}^{15}O$ are displayed. *Upper Right:* Subtraction images indicating the increase in CBF in response to electrical stimulation of the right thumb are superimposed on the MR image (color scale and accompanying percentage represent the increase in CBF). Location of intrinsic optical signals elicited on electrical stimulation of the first and fifth digits are displayed. Different spots close to the central sulcus were activated by stimulations of the different digits (marked as 1 and 5), but the identical area close to the postcentral sulcus was also activated by two digits (marked with an *asterisk*). *Lower Left* and *Center:* The tumor area (yellow), the area with more than 10% increase in CBF on thumb stimulation (red), and the cortical vein (blue) are displayed on MET-PET scans and in the 3D brain surface image, respectively. The increase in CBF was most prominent in the deeper portion of the central sulcus, but the edge of the CBF increase extended to the brain surface. Its location is marked by a *yellow arrow* in the 3D image. *Lower Right:* The location of the intrinsic optical signal in response to thumb stimulation is marked by a *yellow arrow* in the brain surface photograph. Note that the two *black arrows* point out an identical bend of the postcentral gyrus.

people, impairment of the face sensory cortex or the proximal area of the upper or lower extremity will not severely disturb activities of daily living, provided that fine movement of the hand is preserved. In this sense, detailed intraoperative somatotopic mapping obtained with optical imaging is useful to determine the resection border of the sensorimotor cortex by securing the hand area.

In using the optical imaging method, however, we must fully recognize its uses and limitations. One of its limitations is that intrinsic optical signals obtained with 605-nm wavelengths might strongly depend on vascular response and therefore may cause a discrepancy between electrical activities.[27] Our preliminary comparison of imaging intrinsic optical signals, MEG recordings, and PET scanning also revealed such a discrepancy. In an MEG study, we detected the most prominent neuronal activation by somatosensory stimulus of the hand in the postcentral gyrus located deep in the central sulcus, as was represented by our ECD estimation. Although the optical method was not reliable in detecting neuronal activation at this spot, we were successful in detecting an optical signal elicited by somatosensory stimulus at the anterior edge of the central sulcus. The PET CBF activation against somatosensory stimulus of the thumb indicated that the greatest CBF response occurred in the deep portion of the postcentral gyrus, whereas a smaller CBF increase was detected at the edge of the sulcus where the optical signal was detected. As these recordings indicate, the response area detected by methods that depend on focal vascular response, such as imaging of intrinsic optical signals and PET CBF studies, may be broader than electrically detected neuronal activity. Therefore, optical signal mapping may not be used for maximal resection of eloquent cortex but may be used to define the functional border to minimize postoperative functional deficit.

Remember also the physiological correlation between intrinsic optical signals and electrical neuronal activation. Other authors comparing the neuronal response with the optical signal have indicated a rather good correspondence between the two for several seconds after stimulation, as opposed to a rather poor correlation in the later phase after stimulation when the inflow of oxyhemoglobin influences the optical signal.[19,38] These features of optical imaging may

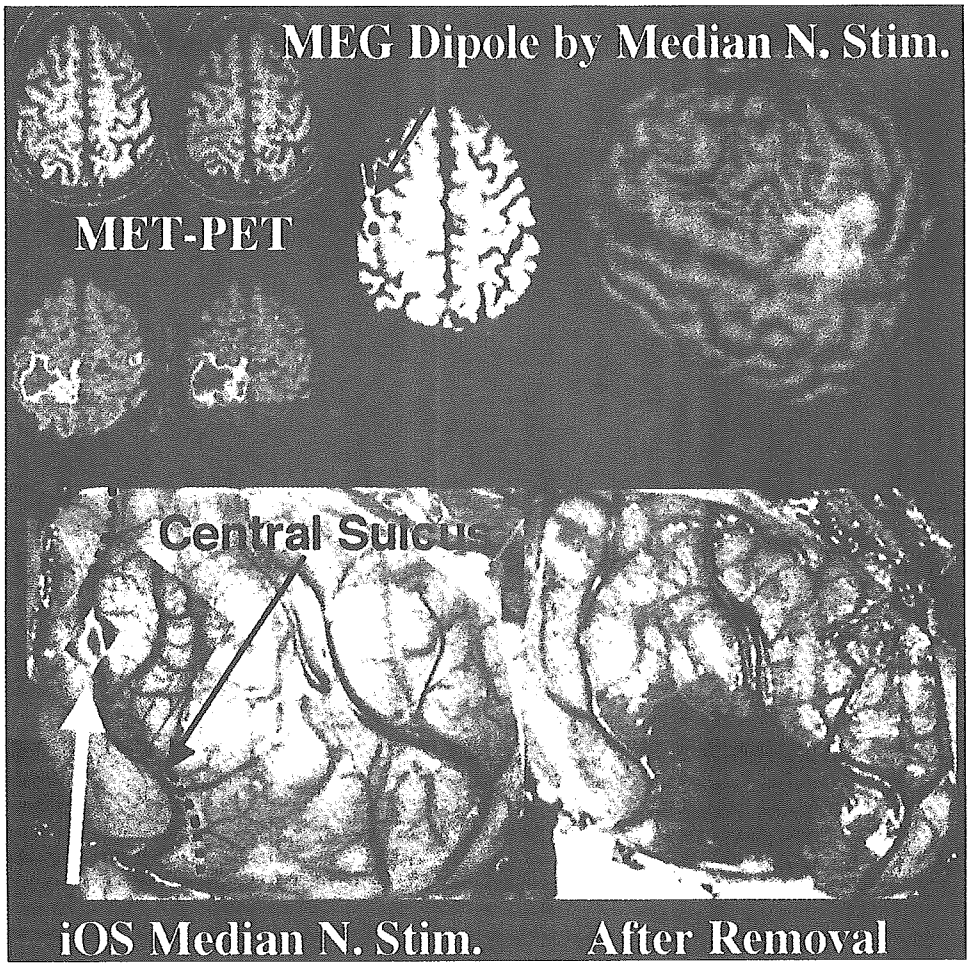

FIG. 6. Case 3. Images obtained before and after surgery for an anaplastic oligodendroglioma in the right postcentral gyrus guided by optical and multimodal imaging. *Upper:* The tumor area was delineated by the increased uptake of MET on PET (MET-PET) and is represented by yellow in the 3D brain surface figures. The MEG ECD was also mapped as a *red spot* to indicate the hand sensory area. *Lower:* Intraoperative recording of intrinsic optical signals (iOS) elicited on median nerve stimulation (N. Stim.) was performed, and the signal was detected on the anterior edge of the postcentral gyrus. The resection margin was set to avoid injuring the cortical area with the hand sensory response, but with the primary sensory cortex medial to this spot (sensory area of the proximal portion of the upper extremity and the entire portion of the lower extremity).

induce responses that do not represent neuronal activation if recording is performed at a different time point after stimulation by using different activation tasks. Therefore, to develop the optical monitoring system to map other brain functions, we need confirmation using electrophysiological or imaging modalities between neuronal activation and optical signal.

We face several practical limitations in using intrinsic optical imaging during surgery. Some of these problems were described in detail in a recent article by other authors.[28] The biggest problem in achieving reliable optical imaging in humans is cortical movement during recording. We solved this problem by inserting a glass plate, as described by others.[14] This method was useful in obtaining reliable somatosensory recordings without injuring the cortical surface, but we cannot ignore the possibility that this procedure influenced the physiological circumstances of cerebral cortex during recording. For widespread clinical use of optical imaging for intraoperative monitoring, commercially available software for noise reduction using an automated image registration technique[4,26,43] is eagerly awaited. Another technical limitation we noticed was as follows: even a small amount of blood in the recording field influences the result. We also experienced a case in which thickened arachnoid membrane interfered with obtaining cortical signals.[34] Because of these two features, optical imaging is difficult to use for a second operation.

Conclusions

Despite these several limitations, intrinsic optical imaging has good potential as a practical and useful monitoring method to delineate the area of human cortical/neuronal activity in images with superior spatial resolution superimposed directly on the actual brain. This method can be used as an intraoperative monitoring tool to localize accurately eloquent cerebral cortex in relation to brain tumors. It might also represent a key method of comparing neuronal activity

detected by electrophysiological recordings and that detected by vascular responses through imaging modalities such as functional MR imaging and PET scanning[5,15,19,29] or of clarifying the significance of noninvasive optical mapping with near-infrared spectroscopy.[10,42]

Acknowledgments

We thank Drs. Itaru Yazawa and Shin-ichi Sasaki for their technical support in the intraoperative recording of optical signals. We also thank Dr. Taketoshi Mehara for his valuable discussions and suggestions.

References

1. Bonhoeffer T, Grinvald A: Iso-orientation domains in cat visual cortex are arranged in pinwheel-like patterns. **Nature 353:** 429–431, 1991
2. Bonhoeffer T, Grinvald A: The layout of iso-orientation domains in area 18 of cat visual cortex: optical imaging reveals a pinwheel-like organization. **J Neurosci 13:**4157–4180, 1993
3. Cannestra AF, Black KL, Martin NA, Cloughesy T, Burton JS, Rubinstein E, et al: Topographical and temporal specificity of human intraoperative optical intrinsic signals. **Neuroreport 9:** 2557–2563, 1998
4. Cannestra AF, Bookheimer SY, Pouratian N, O'Farrell A, Sicotte N, Martin NA, et al: Temporal and topographical characterization of language cortices using intraoperative optical intrinsic signals. **Neuroimage 12:**41–54, 2000
5. Cannestra AF, Pouratian N, Bookheimer SY, Martin NA, Beckerand DP, Toga AW: Temporal spatial differences observed by functional MRI and human intraoperative optical imaging. **Cereb Cortex 11:**773–782, 2001
6. Chapman B, Stryker MP, Bonhoeffer T: Development of orientation preference maps in ferret primary visual cortex. **J Neurosci 16:**6443–6453, 1996
7. Chen-Bee CH, Kwon MC, Masino SA, Frostig RD: Areal extent quantification of functional representations using intrinsic signal optical imaging. **J Neurosci Methods 68:**27–37, 1996
8. Corkin S, Milner B, Rasmussen T: Somatosensory thresholds—contrasting effects of postcentral-gyrus and posterior parietal-lobe excisions. **Arch Neurol 23:**41–58, 1970
9. Dowling JL, Henegar MM, Liu D, Rovainen CM, Woolsey TA: Rapid optical imaging of whisker responses in the rat barrel cortex. **J Neurosci Methods 66:**113–122, 1996
10. Franceschini MA, Boas DA: Noninvasive measurement of neuronal activity with near-infrared optical imaging. **Neuroimage 21:** 372–386, 2004
11. Frostig RD, Lieke EE, Ts'o DY, Grinvald A: Cortical functional architecture and local coupling between neuronal activity and the microcirculation revealed by in vivo high-resolution optical imaging of intrinsic signals. **Proc Natl Acad Sci USA 87:**6082–6086, 1990
12. Godecke I, Bonhoeffer T: Development of identical orientation maps for two eyes without common visual experience. **Nature 379:**251–254, 1996
13. Grinvald A, Lieke E, Frostig RD, Gilbert CD, Wiesel TN: Functional architecture of cortex revealed by optical imaging of intrinsic signals. **Nature 324:**361–364, 1986
14. Haglund MM, Ojemann GA, Hochman DW: Optical imaging of epileptiform and functional activity in human cerebral cortex. **Nature 358:**668–671, 1992
15. Harrison RV, Harel N, Hamrahi H, Panesar J, Mori N, Mount RJ: Local haemodynamic changes associated with neural activity in auditory cortex. **Acta Otolaryngol 120:**255–258, 2000
16. King RB, Shell GR: Cortical localization and monitoring during cerebral operations. **J Neurosurg 67:**210–219, 1987
17. Lehman R, Andermann F, Olivier A, Tandon PN, Quesney LF, Rasmussen TB: Seizures with onset in the sensorimotor face area: clinical patterns and results of surgical treatment in 20 patients. **Epilepsia 35:**1117–1124, 1994
18. LeRoux PD, Berger MS, Haglund MM, Pilcher WH, Ojemann GA: Resection of intrinsic tumors from nondominant face motor cortex using stimulation mapping: report of two cases. **Surg Neurol 36:**44–48, 1991
19. Malonek D, Dirnagl U, Lindauer U, Yamada K, Kanno I, Grinvald A: Vascular imprints of neuronal activity: relationships between the dynamics of cortical blood flow, oxygenation, and volume changes following sensory stimulation. **Proc Natl Acad Sci USA 94:**14826–14831, 1997
20. Masino SA, Kwon MC, Dory Y, Frostig RD: Characterization of functional organization within rat barrel cortex using intrinsic signal optical imaging through a thinned skull. **Proc Natl Acad Sci USA 90:**9998–10002, 1993
21. McCarthy G, Allison T, Spencer DD: Localization of the face area of human sensorimotor cortex by intracranial recording of somatosensory evoked potentials. **J Neurosurg 79:**874–884, 1993
22. Momose-Sato Y, Sato K, Hirota A, Kamino K: GABA-induced intrinsic light-scattering changes associated with voltage-sensitive dye signals in embryonic brain stem slices: coupling of depolarization and cell shrinkage. **J Neurophysiol 79:**2208–2217, 1998
23. Nariai T, Senda M, Ishii K, Maehara T, Wakabayashi S, Toyama H, et al: Three-dimensional imaging of cortical structure, function and glioma for tumor resection. **J Nucl Med 38:**1563–1568, 1997
24. Penfield W, Boldray E: Somatic motor and sensory representation in the cerebral cortex of man as studied by electrical stimulation. **Brain 60:**389–443, 1937
25. Penfield W, Jasper H: **Epilepsy and the Functional Anatomy of the Human Brain.** Boston: Little Brown, 1954, pp 41–155
26. Pouratian N, Bookheimer SY, O'Farrell AM, Sicotte NL, Cannestra AF, Becker D, et al: Optical imaging of bilingual cortical representations. Case report. **J Neurosurg 93:**676–681, 2000
27. Pouratian N, Sheth S, Bookheimer SY, Martin NA, Toga AW: Applications and limitations of perfusion-dependent functional brain mapping for neurosurgical guidance. **Neurosurg Focus 15 (1):**E2, 2003
28. Pouratian N, Sheth SA, Martin NA, Toga AW: Shedding light on brain mapping: advances in human optical imaging. **Trends Neurosci 26:**277–282, 2003
29. Pouratian N, Sicotte N, Rex D, Martin NA, Becker D, Cannestra AF, et al: Spatial/temporal correlation of BOLD and optical intrinsic signals in humans. **Magn Reson Med 47:**766–776, 2002
30. Rumeau C, Tzourio N, Murayama N, Peretti-Viton P, Levrier O, Joliot M, et al: Location of hand function in the sensorimotor cortex: MR and functional correlation. **AJNR 15:**567–572, 1994
31. Sasaki S, Yazawa I, Miyakawa N, Mochida H, Shinomiya K, Kamino K, et al: Optical imaging of intrinsic signals induced by peripheral nerve stimulation in the in vivo rat spinal cord. **Neuroimage 17:**1240–1255, 2002
32. Sato K, Momose-Sato Y, Arai Y, Hirota A, Kamino K: Optical illustration of glutamate-induced cell swelling coupled with membrane depolarization in embryonic brain stem slices. **Neuroreport 8:**3559–3563, 1997
33. Sato K, Nariai T, Sasaki S, Yazawa I, Mochida H, Miyakawa N, et al: Intraoperative intrinsic optical imaging of neuronal activity from subdivisions of the human primary somatosensory cortex. **Cereb Cortex 12:**269–280, 2002
34. Sato K, Nariai T, Tanaka Y, Maehara T, Miyakawa N, Sasaki S, et al: Functional representation of the finger and face in the human somatosensory cortex: intraoperative intrinsic optical imaging. **Neuroimage 25:**1292–1301, 2005
35. Schwartz TH, Chen LM, Friedman RM, Spencer DD, Roe AW: Intraoperative optical imaging of human face cortical topography: a case study. **Neuroreport 15:**1527–1531, 2004
36. Shmuel A, Grinvald A: Functional organization for direction of motion and its relationship to orientation maps in cat area 18. **J Neurosci 16:**6945–6964, 1996

37. Shoham D, Grinvald A: The cortical representation of the hand in macaque and human area S-I: high resolution optical imaging. **J Neurosci 21:**6820–6835, 2001
38. Shtoyerman E, Arieli A, Slovin H, Vanzetta I, Grinvald A: Long-term optical imaging and spectroscopy reveal mechanisms underlying the intrinsic signal and stability of cortical maps in V1 of behaving monkeys. **J Neurosci 20:**8111–8121, 2000
39. Tanaka T, Yazawa I, Sato K, Momose-Sato Y, Kamino K: Consistency behind trial-to-trial variation in intrinsic optical responses to single-whisker movement in the rat D1-barrel cortex. **Neurosci Res 36:**193–207, 2000
40. Toga AW, Cannestra AF, Black KL: The temporal/spatial evolution of optical signals in human cortex. **Cereb Cortex 5:**561–565, 1995
41. Ts'o DY, Frostig RD, Lieke EE, Grinvald A: Functional organization of primate visual cortex revealed by high resolution optical imaging. **Science 249:**417–420, 1990
42. Watanabe E, Yamashita Y, Maki A, Ito Y, Koizumi H: Non-invasive functional mapping with multi-channel near infra-red spectroscopic topography in humans. **Neurosci Lett 205:**41–44, 1996
43. Woods RP, Cherry SR, Mazziotta JC: Rapid automated algorithm for aligning and reslicing PET images. **J Comput Assist Tomogr 16:**620–633, 1992
44. Yazawa I, Sasaki S, Mochida H, Kamino K, Momose-Sato Y, Sato K: Developmental changes in trial-to-trial variations in whisker barrel responses studied using intrinsic optical imaging: comparison between normal and de-whiskered rats. **J Neurophysiol 86:**392–401, 2001
45. Yousry TA, Schmid UD, Alkadhi H, Schmidt D, Peraud A, Buettner A, et al: Localization of the motor hand area to a knob on the precentral gyrus. A new landmark. **Brain 120:**141–157, 1997

Manuscript received August 28, 2004.
Accepted in final form May 4, 2005.
This work was supported by Grants-in-Aid for Scientific Research Grant No. 13470286 from the Ministry of Education, Culture, Sports, Science and Technology, Japan. It was also partially supported by a grant-in-aid from 21st Century COE Project of Ministry of Education, Culture, Sports, Science and Technology awarded to Tokyo Medical and Dental University.
Address reprint requests to: Tadashi Nariai, M.D., Ph.D., Department of Neurosurgery, Tokyo Medical and Dental University, 1-5-45 Yushima, Bunkyo-ku, Tokyo 113–8519, Japan. email: nariai.nsrg@tmd.ac.jp.

J Neurosurg 103:498–507, 2005

Usefulness of L-[methyl-^{11}C] methionine–positron emission tomography as a biological monitoring tool in the treatment of glioma

TADASHI NARIAI, M.D., PH.D., YOJI TANAKA, M.D., HIROAKI WAKIMOTO, M.D., PH.D., MASARU AOYAGI, M.D., PH.D., MASASHI TAMAKI, M.D., PH.D., KIICHI ISHIWATA, PH.D., MICHIO SENDA, M.D., PH.D., KENJI ISHII, M.D., KIMIYOSHI HIRAKAWA, M.D., PH.D., AND KIKUO OHNO, M.D., PH.D

Department of Neurosurgery, Tokyo Medical and Dental University; Positron Medical Center, Tokyo Metropolitan Institute of Gerontology, Tokyo; Department of Neurosurgery, Musashino Red Cross Hospital, Musashino; and Department of Image-Based Medicine, Institute of Biomedical Research and Innovation, Kobe, Japan

Object. The authors retrospectively analyzed the data obtained in patients who had undergone L-[methyl-^{11}C] methionine (MET)–positron emission tomography (PET) studies to clarify the relationship between MET uptake and tumor biological features and to discuss the clinical usefulness of MET-PET studies.

Methods. One hundred ninety-four patients with cerebral glioma or suspected glioma underwent PET scanning 20 minutes after injection of MET, whose uptake into the tumor was expressed as a ratio to contralateral healthy brain tissue (T/N ratio). Analyses were performed to determine how MET uptake correlated with tumor pathological features and prognosis. The T/N ratios before and after various treatments were also examined.

There were significant differences in the T/N ratio among the nonneoplastic lesions, low-grade gliomas, and malignant gliomas. Furthermore, there were significant correlations between patient survival and pretreatment T/N ratios. Among patients with malignant gliomas, a significant difference in survival was observed between cases with and without postoperative tumor remnant based on elevated MET uptake. The MET uptake was heterogeneous even among the homogeneous tumor areas demonstrated on MR imaging. Malignant pathological features were detected in the areas with the highest MET uptake. The effectiveness of radiotherapy or chemotherapy was expressed as a significantly decreased T/N ratio in some of the tumor types.

Conclusions. The ability of MET-PET to reflect the biological nature of gliomas makes it an excellent method for monitoring active tumor tissue, and treatments based on its findings should provide a powerful clinical protocol in the course of glioma therapy.

KEY WORDS • **glioblastoma multiforme** • **astrocytoma** • **oligodendroglioma** • **positron emission tomography** • **amino acid tracer**

THE combination of PET scanning with a radiolabeled amino acid has been proven effective in the diagnosis of glioma. The PET examination of MET uptake has been reported to delineate both benign and malignant glioma more clearly than either enhanced computerized tomography scanning or enhanced MR imaging.[6,22,27,28,38,41] Given that amino acids readily cross the intact BBB through neutral amino acid transporters[35,36] and are incorporated into the area with active tumor,[16] they can be considered suitable for aiding in the diagnosis of disease and for formulating surgical strategies for both low-grade and malignant glial tumors that infiltrate into seemingly healthy cerebral cortex without BBB disruption. Some data have also confirmed the reliability of semiquantitative MET evaluation as a prognostic factor in patients with cerebral glioma.[5,17,29] Thus, we propose that the accurate assessment of tumor biological characteristics and the area of tumor infiltration based on MET-PET imaging should contribute to the treatment of glioma on various occasions.

We have long been using MET-PET images in our neurosurgical clinics for the diagnosis, surgical planning, and postoperative follow up of intracranial gliomas.[24] In the present report, we retrospectively analyzed our cases with respect to tumor pathobiological characteristics and prognosis as well as the effectiveness of surgical and adjuvant therapies to determine how this imaging technique can be applied as a routine clinical modality in the course of glioma treatment.

Abbreviations used in this paper: BBB = blood–brain barrier; CI = confidence interval; FDG = [^{18}F]fluorodeoxyglucose; FLAIR = fluid-attenuated inversion-recovery; KPS = Karnofsky Performance Scale; MET = L-[methyl-^{11}C]methionine; MR = magnetic resonance; OR = odds ratio; PET = positron emission tomography; ROI = region of interest; SUV = standardized uptake value.

Clinical Material and Methods

Patient Population

We analyzed 194 consecutive patients who were strongly suspected of harboring gliomas and underwent MET-PET scanning between January 1992 and December 2002. The MET examinations performed in patients with metasta-

TABLE 1

*Final diagnosis in 194 patients who underwent MET-PET imaging**

Tumor Type	No. of Patients
nonneoplastic lesion	55
radiation necrosis	19
angioma	7
infarct	6
FCD	3
gliosis	3
granuloma	1
trauma	1
meningioangiomatosis	1
unknown	14†
WHO Grade I tumor	12
DNET	5
ganglioglioma	3
central neurocytoma	2
pilocytic astrocytoma	1
Lerhmitte–Duclos disease	1
WHO Grade II tumor	50
astrocytoma	28
oligodendroglioma	21
pleomorphic xanthoastrocytoma	1
WHO Grade III tumor	38
anaplastic astrocytoma	31
anaplastic oligodendroglioma	7
WHO Grade IV tumor	29
GBM	29
other	10
germinoma	2
lymphoma	1
unknown	7

* DNET = dysembryoplastic neuroepithelial tumor; FCD = focal cortical dysplasia.

† Pathological diagnosis was not obtained but assumed to be ischemic lesion, traumatic lesion, FCD, or angioma given that none showed worsening during the 3 to 11 years of follow up.

tic tumors during this same period were excluded. Patients with glioma in the brainstem or bilateral basal ganglia were also excluded because of our inability to obtain tumor uptake values in comparison with the control regions. The final diagnoses in the 194 patients included in the study are listed in Table 1. Of the 129 patients with glioma, 73 underwent surgery at our institutions and were followed up for more than 1 year. Prognoses in these patients were compared with preoperative PET data. The final pathological diagnoses in these 73 patients are listed in Table 2.

Positron Emission Tomography Measurements

We measured equilibrated radioactivity 20 minutes after intravenous injection of MET (250–500 MBq) by using a PET scanner (Headtome IV or V; Shimadzu, Kyoto, Japan). Transmission data were acquired in each patient by using a rotating ^{68}Ge rod source for attenuation correction. Regional uptake of MET was expressed as an SUV ([tissue activity{Bq}/tissue volume {ml}])/([injected radioisotope activity{Bq}/body weight{g}]), and tracer uptake by the tumor was expressed as the ratio of the SUV to the contralateral normal brain (T/N ratio). To determine the tumor's SUV, ROIs were manually placed over the lesion area for a maximum of four axial images. When the lesion was difficult to detect on the PET scan, PET data were registered with MR imaging data so that the tumor could be demonstrated. Image fusion was performed using an automated image analysis program[1] or a manual registration program developed at our institution[32] combined with the Dr. View, version 5.3, image analysis software system (Asahi Kasei Information System Co., Ltd., Tokyo, Japan) on a computer workstation (O2; Silicon Graphics, Inc., Mountain View, CA).

TABLE 2

Pathological diagnoses in 73 patients who were followed up for prognostic analysis

Tumor Type	No. of Patients
Grade I	9
DNET	4
ganglioglioma	3
central neurocytoma	1
Lerhmitte–Duclos disease	1
Grade II	30
astrocytoma	15
oligodendroglioma	14
pleomorphic xanthoastrocytoma	1
Grade III	20
anaplastic astrocytoma	16
anaplastic oligodendroglioma	4
Grade IV	14
GBM	14

To compare precisely the tumor pathological features and regional T/N ratio of MET uptake, the fused PET and MR images constructed with Dr. View were exported to the neuronavigation system (StealthStation; Medtronic Surgical Navigation Technologies, Louisville, CO) used to guide the tissue sampling.

Statistical Analysis

Statistical analyses were performed to compare the T/N ratios among various types of lesions and among groups after different treatments by using analysis of variance and post hoc comparisons with a Bonferroni correction. An analysis of the comparison between prognosis and the T/N ratio of MET uptake was performed using the Kaplan–Meier method with the log-rank test or regression analysis with the proportional hazard model. For all statistics, a probability value less than 0.05 was considered significant. All data are expressed as the means ± standard deviation.

Results

Analysis of Pretreatment Uptake of MET and Tumor Pathological Characteristics

The T/N ratio of MET uptake was analyzed among nonneoplastic lesions and tumors of different grades based on WHO criteria.[18] The results are displayed in Fig. 1. In a statistical comparison of the T/N ratio among five lesion groups (a nonneoplastic group and four tumor groups), all but two of the pairs—Grade I compared with II and Grade III compared with IV—were significantly different; that is, the T/N ratio was proven to differ significantly among three lesion groups: nonneoplastic lesion, low-grade glioma (Grades I and II), and malignant glioma (Grades III and IV).

Analysis of Pretreatment Uptake of MET and Prognosis

Prognoses were analyzed in terms of the pretreatment values of MET uptake. A regression analysis with the pro-

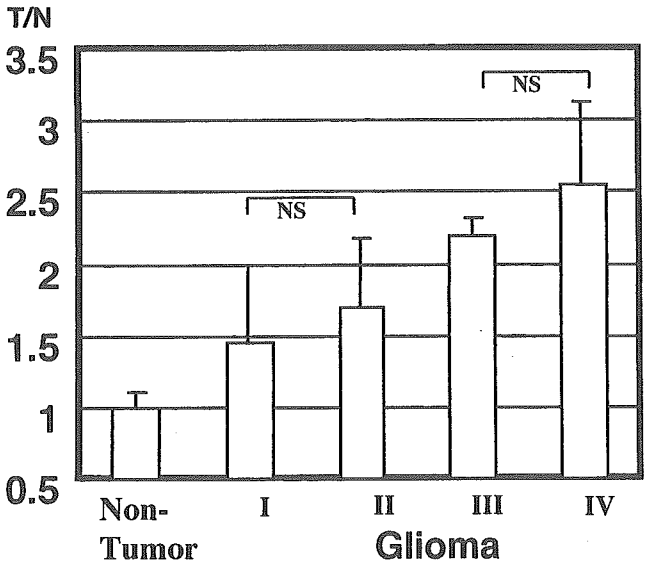

FIG. 1. Bar graph indicating the T/N ratio of MET uptake among nonneoplastic tissue and tumors of different WHO grades (Grades I–IV). A statistical comparison of the T/N ratio among five lesion groups was performed using a Bonferroni correction for multiple comparisons. There were significant differences between all but two of the pairs, that is, Grades I and II, and Grades III and IV (indicated as NS). These findings confirmed significant differences in the T/N ratio among nonneoplastic lesions, low-grade gliomas (Grades I and II), and malignant gliomas (Grades III and IV). NS = not significant.

portional hazard model was used to test the correlation between the survival period after PET scanning and the T/N ratio. Other parameters that could be obtained before surgery, that is, patient age and performance status as expressed by the KPS, were also included in the regression model. The pretreatment T/N ratio of MET uptake and patient age were both found to contribute significantly to patient survival (pretreatment T/N ratio: $p = 0.027$, OR = 1.93, 95% CI 1.07–3.42; patient age: $p = 0.025$, OR = 1.033, 95% CI 1.004–1.064), whereas the KPS did not significantly correlate with the survival period ($p = 0.55$). Figure 2 displays the survival curve calculated using the Kaplan–Meier method for two patient groups: those with high MET uptake and those with low uptake. Patients with a T/N ratio of 1.706 (the median value among all patients) or more were categorized in the high-uptake group and those with a ratio less than 1.706 were categorized in the low-uptake group. A statistically significant difference in the survival period was noted between these two uptake groups ($p = 0.0007$, log-rank test).

Detection of Heterogeneous Pathological Characteristics of Glioma in Each Patient by Using MET-PET Scans

We have been using MET-PET scans coregistered to each patient's own MR imaging data for surgical planning, as reported in a previous article.[24] When used in combination with neuronavigation, this system was useful in precisely comparing the focal T/N ratio of MET uptake with tumor pathological characteristics. By performing these procedures, we often found the heterogeneous characteristics of glioma even in patients with homogeneous findings on MR

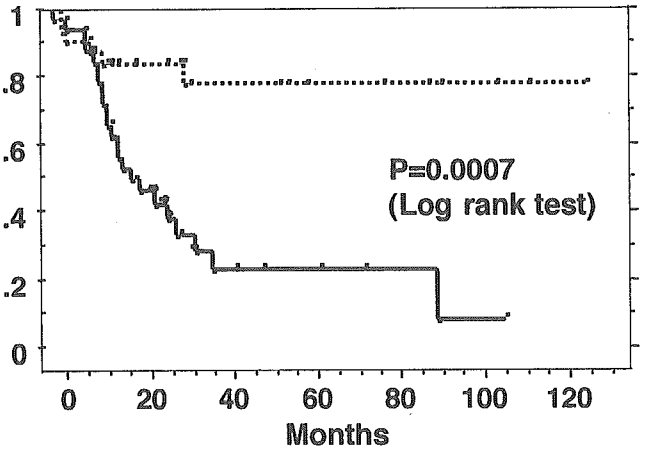

FIG. 2. Graph depicting survival curves drawn using the Kaplan–Meier method for two groups of patients: those with high MET uptake and those with low uptake. The patients were divided based on pretreatment values of the T/N ratio of MET. Patients with a T/N ratio of 1.706 or more were grouped in the high-uptake group (*solid line*, 37 patients, mean age 44.7 ± 15 years) and those with a T/N ratio less than 1.706 were grouped in the low-uptake group (*dotted line*, 36 patients, mean age 39.8 ± 15.7 years). A significant difference in the survival period was noted between the two groups ($p = 0.0007$, log-rank test).

imaging studies. Figures 3 and 4 feature two representative cases in which tissues from areas with highly elevated MET uptake confirmed a final pathological diagnosis of GBM and tissues from areas with lower MET uptake had pathological findings compatible with Grade II astrocytoma. Gadolinium-enhanced T_1-weighted, T_2-weighted, and FLAIR MR images did not depict marked tissue heterogeneity in the tumor area. Another interesting finding was that in most low-grade gliomas and many malignant gliomas, tumor mass was demonstrated on MET-PET scans of the area without contrast enhancement on MR images, as exemplified in cases of GBM (Figs. 3 and 4). Therefore, surgical planning based on MET-PET scanning should be more accurate than that based on MR imaging. Using such PET information, we radically resected the area with elevated MET uptake in the case presented in Fig. 3. In the 5 years since the successful removal of this area with high MET uptake, the patient has been in complete remission with no recurrence of neurological symptoms and neuroradiological findings. In the case presented in Fig. 4, the cortical lesion recurred 18 months after radical resection, but the patient has been able to sustain an active daily life with gamma knife treatment and chemotherapy. No radical treatment was applied to the thalamic regions other than conventional radiation, but no changes on MR or PET images was detected during the follow up of 2 years and 3 months. This follow-up result clearly proved that the malignant tumor cells resided exclusively in the area with highly elevated MET uptake, whereas the low-grade tumor cells resided in the area with only moderately elevated uptake.

Effect of Surgical Treatment Monitored Using MET-PET Scanning

After initial treatment with surgery and conventional radiation, the MET-PET scans obtained in 65 patients with

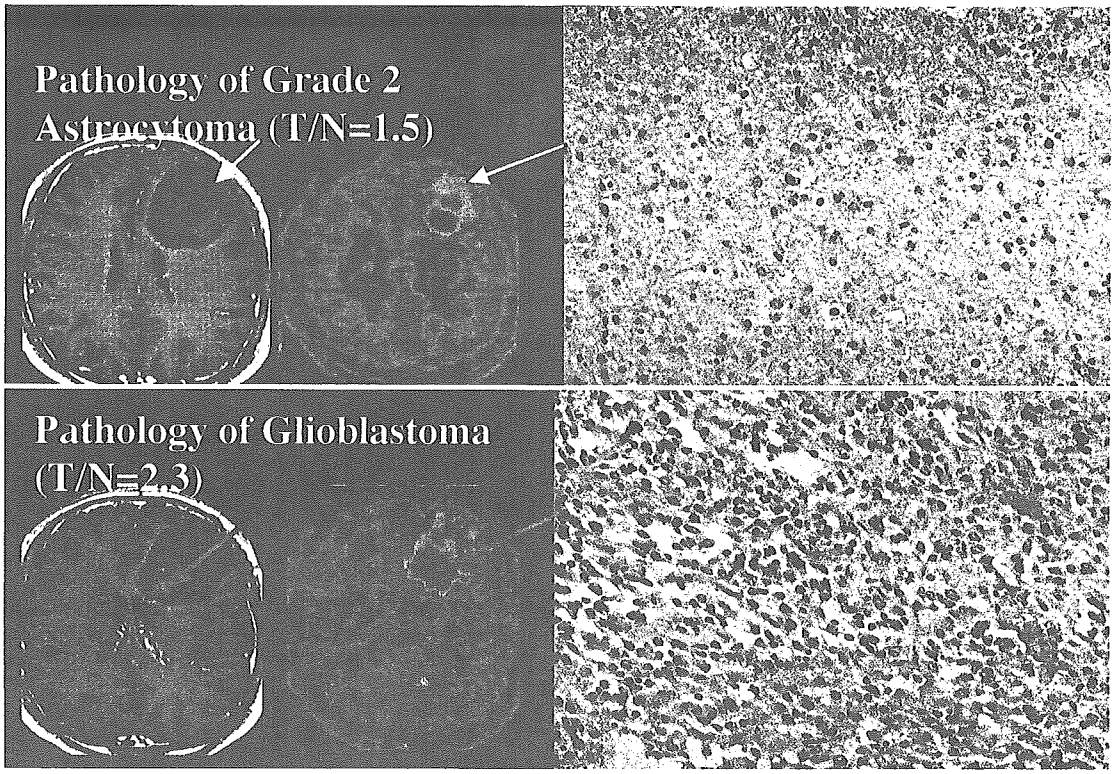

FIG. 3. Images obtained in a 42-year-old man with a lesion in the left frontal lobe. Gadolinium-enhanced T_1-weighted MR images *(left)* demonstrating only mild spotty enhancement in the deep portion. Two MET-PET images superimposed on MR images revealing areas with elevated uptake of MET extending far beyond the area without Gd enhancement. Photomicrographs of tissue from the area with highly elevated MET uptake indicating GBM (indicated with *red arrows*, T/N 2.3), whereas the area with lower MET uptake (indicated with *yellow arrows*, T/N 1.5) had pathological features compatible with Grade II astrocytoma. Original magnification × 400.

Grade II to IV gliomas were evaluated to ascertain whether remnant tumor was present. Thirty-five images demonstrated malignant glioma remnant (Grades III and IV), and 30 Grade II tumor remnant. Patients with Grade I tumor were not included in this analysis because all of them are still alive. A tissue portion with a T/N ratio of more than 1.25 (that is, mean ± two standard deviations of nonneoplastic group presented in Fig. 1) was considered to be a tumor remnant. When a borderline T/N ratio made it difficult to judge the presence of remnant tumor, patients were included in the total resection group. Prognosis was analyzed among patients with an apparent tumor remnant detected through MET uptake, those without a remnant, and those treated without the MET uptake study during the same period. Thirty-one malignant gliomas and six Grade II gliomas were included in the last group.

Our analysis of survival in patients with malignant glioma is shown in Fig. 5. Apparently there was significantly better prognosis in patients without a tumor remnant on MET-PET scanning than in other groups. The survival curve for patients with an apparent tumor mass overlapped that for patients treated without an MET examination. Results of our analysis of survival in patients with Grade II gliomas is shown in Fig. 6. There was no significant difference in survival among the three groups at the end of the 126-month follow up.

From these analyses one could infer that in a maximum follow-up period of approximately 11 years, total resection of an area with elevated MET uptake was beneficial in patients with malignant glioma, whereas the benefit of total resection in patients with Grade II glioma could not be confirmed. Figure 7 shows the results of postoperative MET examination in three representative cases of malignant glioma. The MET-PET images in Fig. 7A are the postoperative figures obtained in the patient with GBM who was also featured in Fig. 3. In the 5 years since resection with no apparent tumor remnant, this patient has remained free from recurrence or neurological deficit. Positron emission tomography scans obtained in the patient in Fig. 7B, whose anaplastic astrocytoma was thought to be totally resected based on Gd-enhanced MR imaging, revealed a broad area of elevated MET uptake in the basal ganglia in the same week that the MR imaging studies had been performed. New Gd-enhanced lesions appeared in this same area together with left hemiparesis 3 months later. An MR image also indicated total resection of the GBM in the patient represented in Fig. 7C, whereas an MET-PET scan obtained in the same week clearly demonstrated active tumor mass in the basal ganglia and the other side of brain. A new Gd-enhanced lesion appeared in this area 3 months later.

Effect of Adjuvant Therapy Monitored With MET-PET Images

A total of 51 MET-PET scans were obtained after administering radiation therapy alone or in combination with che-

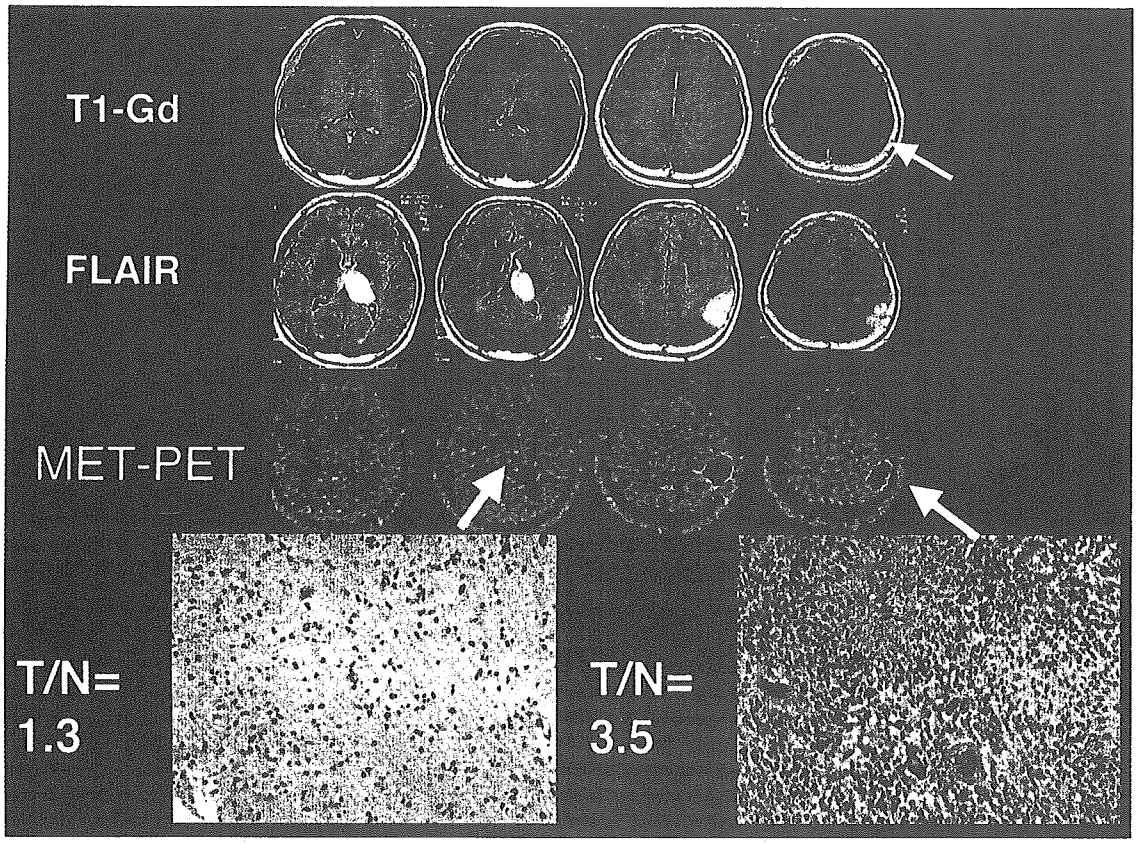

FIG. 4. Gadolinium-enhanced T_1-weighted and FLAIR MR images, MET-PET images, and photomicrographs obtained in a 40-year-old man with lesions in the left thalamus and parietal cortex. The FLAIR MR images exhibited homogeneous enhancement in these lesions. Only a small enhanced spot was noted in the parietal cortex (indicated by the *yellow arrow*). No interregional heterogeneity was apparent on MR imaging, whereas marked regional heterogeneity was detected on MET-PET. Photomicrographs demonstrating tissue from the parietal cortex with highly elevated MET uptake (T/N 3.5, *right*) was pathologically diagnosed as GBM, whereas a biopsy specimen of the thalamus, a brain portion with only mildly elevated MET uptake (T/N 1.3, *left*), revealed pathological features compatible with Grade II astrocytoma. Note that almost all of the GBM tissue was obtained in the area without Gd enhancement. Original magnification × 400.

motherapy against remnant tumors. After grouping patients according to their lesion type (that is, Grade II astrocytoma, Grade III astrocytoma, GBM, and tumors with an oligodendroglial component [oligodendroglioma, oligoastrocytoma, and anaplastic oligodendroglioma]), the T/N ratios of the radiation group and the radiation plus chemotherapy group were compared with pretreatment values among tumors of the same pathological type (Fig. 8).

Patients with anaplastic astrocytoma and GBM had significantly decreased postradiation T/N ratios compared with pretreatment values, but there was no significant difference between ratios in the radiation and radiation plus chemotherapy groups. Gliomas with oligodendroglial components in the radiation plus chemotherapy group had significantly decreased T/N ratios compared with those in the radiation group and the pretreatment value. In the case of Grade II astrocytomas, the T/N ratios of the radiation group and radiation plus chemotherapy group were not significantly different from the pretreatment values. Figure 9 features a case of GBM after radiation therapy in which part of the lesion that had enhanced on MR imaging represented an active tumor mass, whereas the other part represented necrotic tissue.

Discussion

Many cases of cerebral glioma are still incurable despite recent advances in neuroimaging, neurosurgical techniques, and various adjuvant therapies. Part of the problem is the tendency of most glial tumors to infiltrate into seemingly healthy brain tissue.[8,23] When this happens, the tumors are often difficult to localize using imaging techniques based mainly on areas of disrupted BBB detected by the leakage of intravenously injected contrast medium. Gliomas are especially difficult to delineate when the BBB is further disrupted because of an operation or radiation therapy. These factors often make it difficult even to monitor the effectiveness of individual therapies by conventional imaging studies. One solution that could benefit glioma treatment would be a tomographic imaging method with a radiolabeled tracer that crosses the intact BBB and accumulates into the area, with glioma infiltration reflecting the biological nature of the tumor with good contrast to surrounding brain. The FDG-PET method, now widely used for whole-body tumor imaging,[4,9] seems to work in just this way. Unfortunately, however, high uptake of FDG in healthy brain tissue has been reported to hamper tumor imaging, especially when the lesion type is not highly malignant.[19,27]

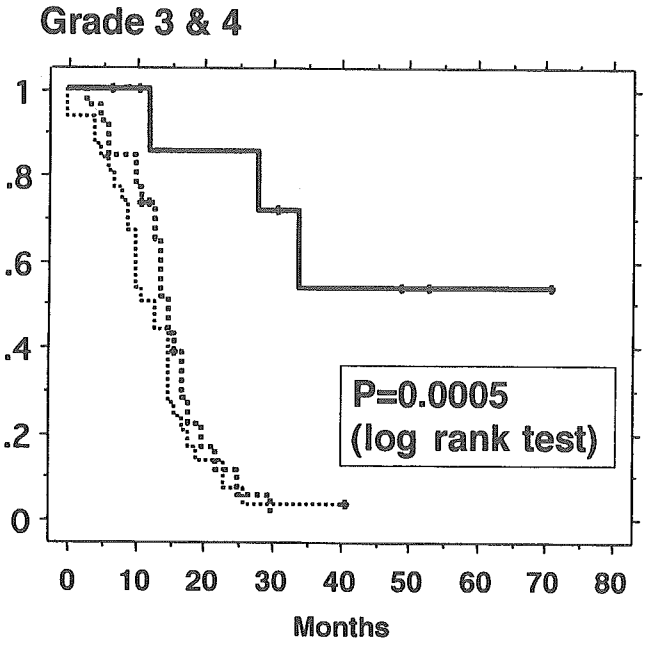

FIG. 5. Graph depicting survival curves drawn using the Kaplan–Meier method for three groups of patients with malignant glioma (Grades III and IV): patients without areas of elevated MET uptake after initial treatment (*solid line*, eight patients, mean age 43.4 ± 15.5 years; three GBMs, four anaplastic astrocytomas, one anaplastic oligodendroglioma), those with areas of elevated MET uptake after initial treatment (*bold dotted line*, 27 patients, mean age 48.6 ± 15 years; 11 GBMs, 13 anaplastic astrocytomas, three anaplastic oligodendrogliomas), and those who did not undergo MET-PET imaging (*dotted line*, 31 patients, mean age 53.9 ± 13.8 years; 24 GBMs, five anaplastic astrocytomas, two anaplastic oligodendrogliomas). A significant difference in the survival period was noted among the three groups ($p = 0.0005$, log-rank test), and the group without MET detection of remnant tumor had a significantly better prognosis than the others.

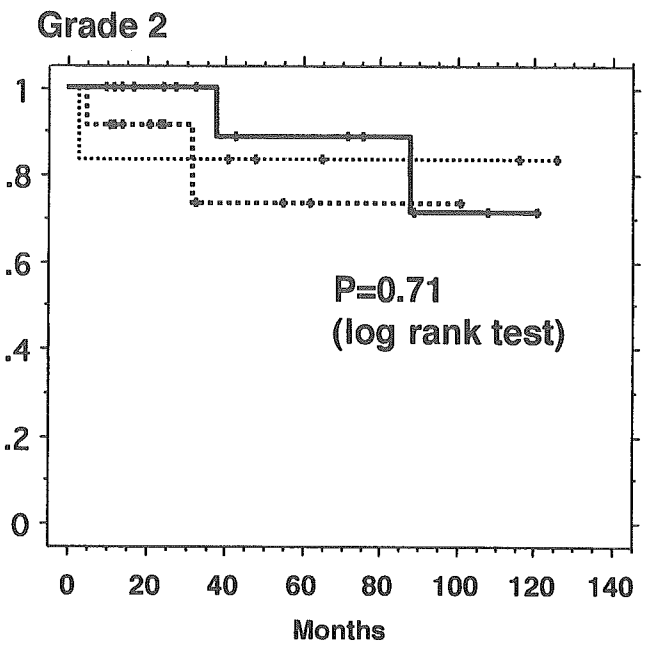

FIG. 6. Graph depicting survival curves drawn using the Kaplan–Meier method for three groups of patients with Grade II glioma: patients without areas of elevated MET uptake after initial treatment (*solid line*, 18 patients, mean age 39.4 ± 11.6 years; nine astrocytomas, eight oligodendrogliomas, one pleomorphic xanthoastrocytoma), those with areas of elevated MET uptake after initial treatment (*bold dotted line*, 12 patients, mean age 44.5 ± 13.4 years; six astrocytomas, six oligodendrogliomas), and those who did not undergo MET-PET imaging (*dotted line*, six patients, mean age 32.5 ± 12.5 years; six astrocytomas). No significant difference in the survival period was noted among the three groups ($p = 0.71$, log-rank test).

In contrast, radiolabeled amino acid has been identified as a suitable imaging probe for both low-grade and malignant gliomas given that, compared with FDG, less of the amino acid tracer is taken up in the healthy brain. Among the various amino acid tracers,[16] MET is used in most clinical studies of brain tumor because of its simple and efficient labeling characteristics. Our group uses MET for the accurate delineation of gliomas for surgical treatment,[24] and more recently we have adopted the technique for use during the entire glioma treatment course. Our clinical experience and other previously reported data strongly indicate that MET-PET scanning is an excellent method for localizing and characterizing glial tumors.[5–7,11,12,29]

The original premise of amino acid imaging was the quantification of protein synthesis in vivo,[13,33,34] and certain types of amino acid tracer combined with PET scanning have proven effective for this use.[15,41] Note, however, that the metabolism of MET is complicated and has been reported to reflect both protein synthesis and the blood–brain transport of tracer at the same time.[14] Thus, the significance of MET uptake is difficult to interpret solely in the context of kinetic analysis. Nonetheless, a retrospective analysis of MET data supported by accurate data on tumor pathological features and patient outcome is extremely valuable in establishing a guideline for the routine clinical use of MET-PET imaging.

In the present report we showed that a comparatively expressed MET uptake ratio accurately reflected the biological nature of glioma. There were significant differences in the uptake ratio among patients harboring nonneoplastic lesions, low-grade gliomas, and malignant gliomas. The uptake ratios recorded before treatment were highly correlated with prognosis. Results of a comparison between focal MET uptake and tumor pathological features indicated that malignant portions of lesions could be found in the areas with the greatest MET uptake. All of these findings attest to the reliability of the MET-PET image as a marker of tumor biological characteristics.

Data in the present study also demonstrated the utility of MET-PET imaging in monitoring the effectiveness of treatment. A remnant of malignant glioma was often detected with MET after initial treatment even when MR imaging had revealed no such lesion, and the patients in whom this occurred faced a significantly poorer prognosis than the cases with no remnant mass on MET-PET studies. In patients with malignant glioma, this circumstance led us to believe that MET can provide useful guidelines for maximal resection in the operating room. In the actual clinical setting, however, malignant tumor mass was preoperatively

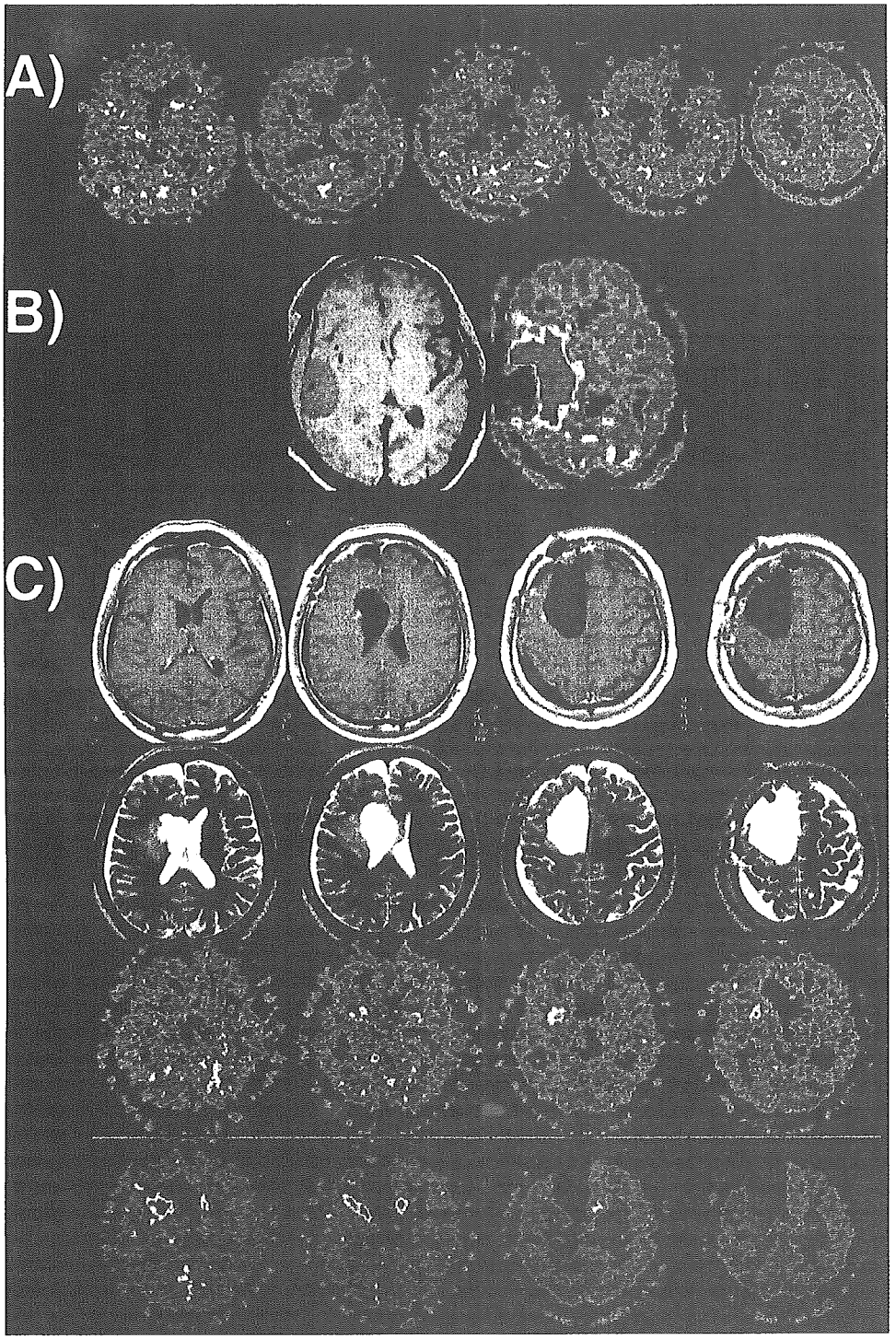

FIG. 7. A: Postoperative MET-PET images obtained in a 42-year-old man with a left frontal GBM whose preoperative images are featured in Fig. 3. No apparent tumor remnant was detected on the MET-PET images. The patient has remained free from recurrence during the 55-month follow up since this scan. B: Postoperative Gd-enhanced T_1-weighted *(left)* and MET-PET *(right)* images obtained in the same week in a 54-year-old woman with anaplastic astrocytoma. No apparent tumor remnant was demonstrated on the Gd-enhanced MR image, whereas the MET-PET study revealed a large tumor mass in the basal ganglia; at this time the patient was asymptomatic. Three months later, MR images revealed new enhancements in the basal ganglia and the patient demonstrated left hemiparesis. C: Postoperative Gd-enhanced T_1-weighted MR *(first row)*, T_2-weighted MR *(second row)*, and MET-PET *(lower two rows)* images obtained in the same week in a 46-year-old man with GBM. No apparent tumor remnant was revealed on the MR images, whereas the MET-PET images demonstrated a tumor remnant in the right basal ganglia and invasion into the contralateral frontal lobe through the corpus callosum. Gadolinium-enhanced lesions appeared in these areas 3 months later.

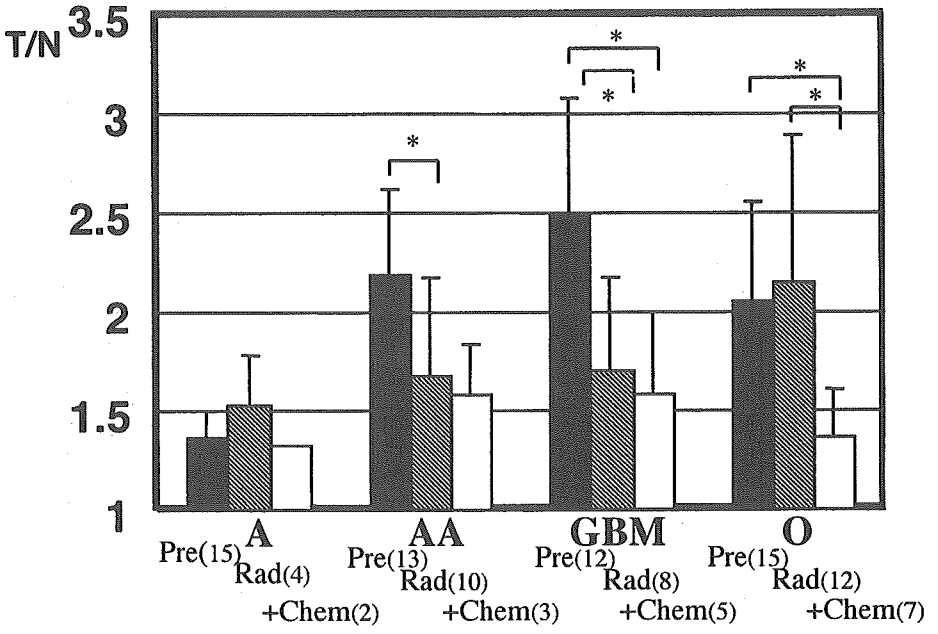

FIG. 8. Bar graph indicating the T/N ratio of MET uptake among four categories of remnant tumor after radiation (Rad, *hatched bar*) and radiation plus chemotherapy (+Chem, *white bar*) compared with pretreatment values (Pre, *black bar*). The number of patients in each group is indicated in parentheses. An *asterisk* indicates a significant difference ($p < 0.05$). A = astrocytoma; AA = anaplastic astrocytoma; O = tumor with oligodendroglial component (oligodendroglioma, oligoastrocytoma, and anaplastic oligodendroglioma).

detected by MET-PET in nonresectable portions such as the basal ganglia, contralateral brain, or eloquent cerebral cortex. Complete mass reduction was achieved based on MET-PET studies in only eight of 35 patients in the present study (Fig. 5). The only solution for this problem may be the early detection of glioma with MET-PET imaging combined with surgical planning. The technique of MET-PET imaging will prove useful for this purpose once it is used more frequently on a daily clinical basis. In interpreting the results of this survival analysis, however, we must exercise caution. This study is a retrospective analysis and the patient groups were not homogeneous. More GBMs were included in the remnant group than in the total resection group, presumably because of the invasive nature of GBM, and therefore this analysis may be influenced more by the preoperative state than by the treatment effect itself.

We also expected a strong benefit from maximal resection of Grade II gliomas, but there was no significant difference in the survival rate between cases in which the remnant tumor was detected on MET-PET and those in which it was not (Fig. 6). This conclusion was based on data collected over a maximum follow-up period of 11 years. In the case of low-grade tumors, we may need longer follow ups to confirm whether the maximum resection based on MET-PET images benefits the patients. Concerning the MET-PET imaging of low-grade glioma, note that the T/N ratios in four patients with Grade II lesions who died during the follow-up period were 3.2, 1.71, 1.45, and 1.36; thus, two of four ratios exceeded the median value (1.706) among all patients, and 3.2 was the highest value among all patients with low-grade glioma. Longer follow ups are needed to show whether the T/N ratio of MET uptake can be an indicator of low-grade glioma prognosis.

We also analyzed the possible benefit of MET studies in monitoring the effect of adjuvant therapy for remnant tumor. A decrease in MET uptake was recorded after applying conventional radiation for anaplastic astrocytoma and GBM,[20,25,30] and after chemotherapy for glioma with oligodendroglial components.[3,18,31,37] These results correspond well with the effective adjuvant therapy protocol already established. Precise monitoring of treatment effects is an inevitable necessity especially when attempting to develop new therapeutic protocols for incurable diseases like malignant glioma. Unfortunately, however, it often is difficult to judge the effectiveness of a therapy by neurological examination and conventional computerized tomography scanning or MR imaging with contrast medium. Even when neurological symptoms worsen and brain edema and enhancement both increase, we cannot determine whether these changes are signs of tumor progression due to the ineffectiveness or neurotoxic effect of therapy. By observing MET-PET images and tracer uptake expressed by the T/N ratio, we can semiquantitatively assess the tumoricidal effect of treatment.

Note that MET-PET imaging has been reported to be effective in differentiating the recurrence of tumor from radiation necrosis.[39] In the case of malignant glioma, however, neurosurgeons seldom face total radiation necrosis or total recurrence in the course of treatment. Far more common is the appearance of radiation effects in some parts of the brain in combination with progression in other parts at the same time, as demonstrated in the case presented in Fig. 9. Although the application of stereotactic radiotherapy for malignant glioma has been considered,[21,26] such a focal treatment strategy should always be coupled with precise judgment of the focal biological nature of the glioma. The

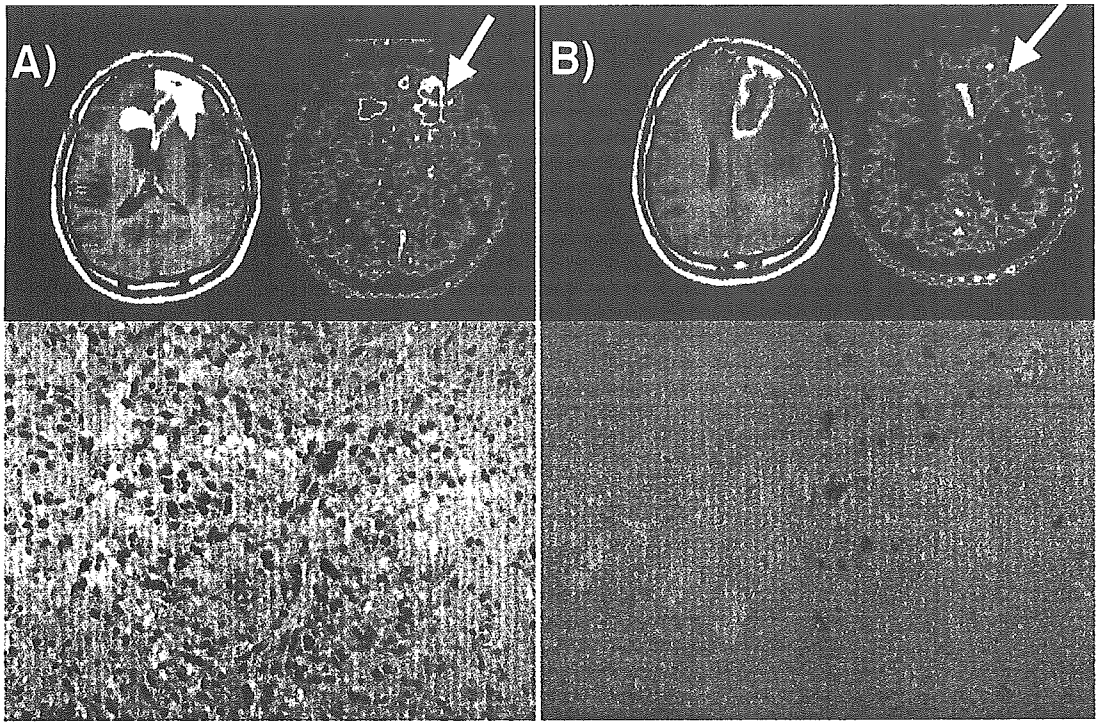

FIG. 9. Gadolinium-enhanced T_1-weighted MR *(left)* and MET-PET *(right)* images as well as photomicrographs *(lower)* of pathological specimens obtained in a 28-year-old man with GBM. This specimen was obtained at the second operation, which was performed when enhancement enlarged following the administration of radiation. A: Pathological specimen obtained from the area of highly elevated uptake of MET, demonstrating active tumor. B: Pathological specimen obtained from the area with MET uptake equivalent to that in surrounding brain, demonstrating mainly necrotic tissue with scattered tumor cells. Tissue sampling was performed using MET-PET images and a neuronavigator. Original magnification × 400.

use of MET-PET can provide for such judgment in the clinical setting.

In the present study, we retrospectively analyzed the results of MET-PET scanning and demonstrated the usefulness of the imaging method for many aspects of glioma therapy. In the next step, we must determine whether we can ameliorate the glioma prognosis by using this modality prospectively. For that purpose, we must establish a clinical environment in which MET-PET is used routinely during the entire course of glioma treatment, that is, from initial diagnosis to surgical planning and periodical follow up during adjuvant therapy. The routine clinical use of FDG-PET studies has been accepted as an effective imaging protocol for systemic cancer. For neurosurgeons, the acceptance of MET-PET imaging as a routine clinical protocol is anticipated. One disadvantage of MET is its unsuitability for commercial distribution given the very short half-life of carbon-11. The development of ^{18}F-labeled amino acid tracer and a clinical study to examine its usefulness may be helpful in making this excellent imaging method available in many clinical institutions.[2,10,40] The use of PET imaging with appropriate amino acid probes such as MET should significantly improve the daily treatment of malignant glioma and encourage the development of new treatment strategies against one of the representative incurable human diseases.

Conclusions

The ability of MET-PET imaging to reflect the biological nature of gliomas makes it an excellent method for monitoring active tumor tissue. Routine clinical use of this technique and treatments based on its findings should provide a powerful clinical protocol in the course of glioma therapy.

References

1. Ardekani BA, Braun M, Hutton BF, Kanno I, Iida H: A fully automatic multimodality image registration algorithm. **J Comput Assist Tomogr 19:**615–623, 1995
2. Becherer A, Karanikas G, Szabo M, Zettinig G, Asenbaum S, Marosi C, et al: Brain tumour imaging with PET: a comparison between [18F]fluorodopa and [11C]methionine. **Eur J Nucl Med Mol Imaging 30:**1561–1567, 2003
3. Buckner JC, Gesme D Jr, O'Fallon JR, Hammack JE, Stafford S, Brown PD, et al: Phase II trial of procarbazine, lomustine, and vincristine as initial therapy for patients with low-grade oligodendroglioma or oligoastrocytoma: efficacy and associations with chromosomal abnormalities. **J Clin Oncol 21:**251–255, 2003
4. Coleman RE: Value of FDG-PET scanning in management of lung cancer. **Lancet 359:**1361–1362, 2002
5. De Witte O, Goldberg I, Wikler D, Rorive S, Damhaut P, Monclus M, et al: Positron emission tomography with injection of methionine as a prognostic factor in glioma. **J Neurosurg 95:**746–750, 2001
6. Derlon JM, Bourdet C, Bustany P, Chatel M, Theron J, Darcel F, et al: [11C]L-methionine uptake in gliomas. **Neurosurgery 25:** 720–728, 1989
7. Derlon JM, Chapon F, Noel MH, Khouri S, Benali K, Petit-Taboue MC, et al: Non-invasive grading of oligodendrogliomas:

correlation between in vivo metabolic pattern and histopathology. **Eur J Nucl Med 27:**778–787, 2000
8. Giese A, Westphal M: Glioma invasion in the central nervous system. **Neurosurgery 39:**235–252, 1996
9. Gould MK, Maclean CC, Kuschner WG, Rydzak CE, Owens DK: Accuracy of positron emission tomography for diagnosis of pulmonary nodules and mass lesions: a meta-analysis. **JAMA 285:** 914–924, 2001
10. Heiss P, Mayer S, Herz M, Wester HJ, Schwaiger M, Senekowitsch-Schmidtke R: Investigation of transport mechanism and uptake kinetics of O-(2–[18F]fluoroethyl)-L-tyrosine in vitro and in vivo. **J Nucl Med 40:**1367–1373, 1999
11. Herholz K, Holzer T, Bauer B, Schroder R, Voges J, Ernestus RI, et al: 11C-methionine PET for differential diagnosis of low-grade gliomas. **Neurology 50:**1316–1322, 1998
12. Holzer T: The in vivo metabolic pattern of low-grade brain gliomas: a positron emission tomographic study using f-18-fluorodeoxyglucose and c-11-L-methylmethionine. **Neurosurgery 42:** 1200–1201, 1998
13. Ingvar MC, Maeder P, Sokoloff L, Smith CB: Effects of ageing on local rates of cerebral protein synthesis in Sprague-Dawley rats. **Brain 108:**155–170, 1985
14. Ishiwata K, Kubota K, Murakami M, Kubota R, Sasaki T, Ishii S, et al: Re-evaluation of amino acid PET studies: can the protein synthesis rates in brain and tumor tissues be measured in vivo? **J Nucl Med 34:**1936–1943, 1993
15. Ishiwata K, Vaalburg W, Elsinga PH, Paans AM, Woldring MG: Metabolic studies with L-[1–14C]tyrosine for the investigation of a kinetic model to measure protein synthesis rates with PET. **J Nucl Med 29:**524–529, 1988
16. Jager PL, Vaalburg W, Pruim J, de Vries EG, Langen KJ, Piers DA: Radiolabeled amino acids: basic aspects and clinical applications in oncology. **J Nucl Med 42:**432–445, 2001
17. Kim S, Chung JK, Im SH, Jeong JM, Lee DS, Kim DG, et al: 11C-methionine PET as a prognostic marker in patients with glioma: comparison with (18)F-FDG PET. **Eur J Nucl Med Mol Imaging 32:**52–59, 2004
18. Kristof RA, Neuloh G, Hans V, Deckert M, Urbach H, Schlegel U, et al: Combined surgery, radiation, and PCV chemotherapy for astrocytomas compared to oligodendrogliomas and oligoastrocytomas WHO grade III. **J Neurooncol 59:**231–237, 2002
19. Kubota K: From tumor biology to clinical PET: a review of positron emission tomography (PET) in oncology. **Ann Nucl Med 15:**471–486, 2001
20. Levin VA, Maor MH, Thall PF, Yung WK, Bruner J, Sawaya R, et al: Phase II study of accelerated fractionation radiation therapy with carboplatin followed by vincristine chemotherapy for the treatment of glioblastoma multiforme. **Int J Radiat Oncol Biol Phys 33:**357–364, 1995
21. Loeffler JS, Alexander E III, Shea WM, Wen PY, Fine HA, Kooy HM, et al: Radiosurgery as part of the initial management of patients with malignant gliomas. **J Clin Oncol 10:**1379–1385, 1992
22. Mineura K, Sasajima T, Suda Y, Kowada M, Shishido F, Uemura K: Amino acid study of cerebral gliomas using positron emission tomography—analysis of (11C-methyl)-L-methionine uptake index. **Neurol Med Chir 30:**997–1002, 1990
23. Nagano N, Sasaki H, Aoyagi M, Hirakawa K: Invasion of experimental rat brain tumor: early morphological changes following microinjection of C6 glioma cells. **Acta Neuropathol 86:** 117–125, 1993
24. Nariai T, Senda M, Ishii K, Maehara T, Wakabayashi S, Toyama H, et al: Three-dimensional imaging of cortical structure, function and glioma for tumor resection. **J Nucl Med 38:**1563–1568, 1997
25. Nelson DF, Curran WJ Jr, Scott C, Nelson JS, Weinstein AS, Ahmad K, et al: Hyperfractionated radiation therapy and bis-chloroethyl nitrosourea in the treatment of malignant glioma—possible advantage observed at 72.0 Gy in 1.2 Gy B.I.D. fractions: report of the Radiation Therapy Oncology Group Protocol 8302. **Int J Radiat Oncol Biol Phys 25:**193–207, 1993
26. Nwokedi EC, DiBiase SJ, Jabbour S, Herman J, Amin P, Chin LS: Gamma knife stereotactic radiosurgery for patients with glioblastoma multiforme. **Neurosurgery 50:**41–47, 2002
27. Ogawa T, Inugami A, Hatazawa J, Kanno I, Murakami M, Yasui N, et al: Clinical positron emission tomography for brain tumors: comparison of fluorodeoxyglucose F 18 and L-methyl-11C-methionine. **AJNR 17:**345–353, 1996
28. Ogawa T, Shishido F, Kanno I, Inugami A, Fujita H, Murakami M, et al: Cerebral glioma: evaluation with methionine PET. **Radiology 186:**45–53, 1993
29. Ribom D, Eriksson A, Hartman M, Engler H, Nilsson A, Langstrom B, et al: Positron emission tomography (11)C-methionine and survival in patients with low-grade gliomas. **Cancer 92:** 1541–1549, 2001
30. Salazar OM, VanHoutte PJ, Bennett JM, Rubin P, Wheeler KT: High-dose radiation therapy with low-dose (pulsed) BCNU in malignant gliomas: an Eastern Cooperative Oncology Group (ECOG) report. **Int J Radiat Oncol Biol Phys 8:**915–919, 1982
31. Schiff D: Dramatic response to chemotherapy in oligodendroglial gliomatosis cerebri. **Neurology 61:**425, 2003
32. Senda M: Mapping cortical functions using PET activation technique, in Sugishita M (ed): **New Horizons in Neuropsychology.** Amsterdam: Elsevier Science, 1994, pp 23–34
33. Smith CB, Crane AM, Kadekaro M, Agranoff BW, Sokoloff L: Stimulation of protein synthesis and glucose utilization in the hypoglossal nucleus induced by axotomy. **J Neurosci 4:**2489–2496, 1984
34. Smith CB, Deibler GE, Eng N, Schmidt K, Sokoloff L: Measurement of local cerebral protein synthesis in vivo: influence of recycling of amino acids derived from protein degradation. **Proc Nat Acad Sci USA 85:**9341–9345, 1988
35. Smith QR, Momma S, Aoyagi M, Rapoport SI: Kinetics of neutral amino acid transport across the blood-brain barrier. **J Neurochem 49:**1651–1658, 1987
36. Smith QR, Takasato Y: Kinetics of amino acid transport at the blood-brain barrier studied using an in situ brain perfusion technique. **Ann NY Acad Sci 481:**186–201, 1986
37. Soffietti R, Ruda R, Bradac GB, Schiffer D: PCV chemotherapy for recurrent oligodendrogliomas and oligoastrocytomas. **Neurosurgery 43:**1066–1073, 1998
38. Tovi M, Lilja A, Bergstrom M, Ericsson A, Bergstrom K, Hartman M: Delineation of gliomas with magnetic resonance imaging using Gd-DTPA in comparison with computed tomography and positron emission tomography. **Acta Radiol 31:**417–429, 1990
39. Tsuyuguchi N, Sunada I, Iwai Y, Yamanaka K, Tanaka K, Takami T, et al: Methionine positron emission tomography of recurrent metastatic brain tumor and radiation necrosis after stereotactic radiosurgery: is a differential diagnosis possible? **J Neurosurg 98:** 1056–1064, 2003
40. Wester HJ, Herz M, Weber W, Heiss P, Senekowitsch-Schmidtke R, Schwaiger M, et al: Synthesis and radiopharmacology of O-(2–[18F]fluoroethyl)-L-tyrosine for tumor imaging. **J Nucl Med 40:**205–212, 1999
41. Willemsen AT, van Waarde A, Paans AM, Pruim J, Luurtsema G, Go KG, et al: In vivo protein synthesis rate determination in primary or recurrent brain tumors using L-[1–11C]-tyrosine and PET. **J Nucl Med 36:**411–419, 1995

Manuscript received December 2, 2004.
Accepted in final form May 26, 2005.
This work was partially supported by a grant-in-aid from 21st Century COE Project of Ministry of Education, Culture, Sports, Science and Technology to Tokyo Medical and Dental University.

Address reprint requests to: Tadashi Nariai, M.D., Ph.D., Department of Neurosurgery, Tokyo Medical and Dental University, 1-5-45 Yushima, Bunkyo-ku, Tokyo 113 Japan. email: nariai.nsrg@tmd.ac.jp.

Available online at www.sciencedirect.com
SCIENCE DIRECT
Nuclear Medicine and Biology 32 (2005) 831–836
NUCLEAR MEDICINE — AND — BIOLOGY
www.elsevier.com/locate/nucmedbio

Greater adenosine A_{2A} receptor densities in cardiac and skeletal muscle in endurance-trained men: a [^{11}C]TMSX PET study

Masaki Mizuno[a,b], Yuichi Kimura[b,*], Ken Tokizawa[c], Kenji Ishii[b], Keiichi Oda[b], Toru Sasaki[b], Yoshio Nakamura[a], Isao Muraoka[a], Kiichi Ishiwata[b]

[a]*Faculty of Sport Sciences, Waseda University, Tokorozawa, Saitama 359-1192, Japan*
[b]*Positron Medical Center, Tokyo Metropolitan Institute of Gerontology, Itabashi-ku, Tokyo 173-0022, Japan*
[c]*Graduate School of Human Sciences, Waseda University, Tokorozawa, Saitama 359-1192, Japan*

Received 11 May 2005; received in revised form 23 June 2005; accepted 1 July 2005

Abstract

We examined the densities of adenosine A_{2A} receptors in cardiac and skeletal muscles between untrained and endurance-trained subjects using positron emission tomography (PET) and [7-*methyl*-^{11}C]-(*E*)-8-(3,4,5-trimethoxystyryl)-1,3,7-trimethylxanthine ([^{11}C]TMSX), a newly developed radioligand for mapping adenosine A_{2A} receptors. Five untrained and five endurance-trained subjects participated in this study. The density of adenosine A_{2A} receptors was evaluated as the distribution volume of [^{11}C]TMSX in cardiac and triceps brachii muscles in the resting state using PET. The distribution volume of [^{11}C]TMSX in the myocardium was significantly greater than in the triceps brachii muscle in both groups. Further, distribution volumes [^{11}C]TMSX in the trained subjects were significantly grater than those in untrained subjects (myocardium, 3.6±0.3 vs. 3.1±0.4 ml g^{-1}; triceps brachii muscle, 1.7±0.3 vs. 1.2±0.2 ml g^{-1}, respectively). These results indicate that the densities of adenosine A_{2A} receptors in the cardiac and skeletal muscles are greater in the endurance-trained men than in the untrained men.
© 2005 Elsevier Inc. All rights reserved.

Keywords: Adenosine A_{2A} receptor; Training; Skeletal muscle; Heart; Human; Positron emission tomography

1. Introduction

Adenosine is an endogenous modulator of several physiological functions in the central nervous system [1] as well as in peripheral organs [2]. The effects are mediated by at least four receptor subtypes: A_1, A_{2A}, A_{2B} and A_3 [3]. In particular, adenosine A_{2A} receptors may contribute to some physiological functions in cardiac and skeletal muscle. In myocardium, these receptors may involve an acquisition of the resistance to ischemia [4,5] and may modulate contraction [6,7]. By contrast, adenosine A_{2A} receptors in skeletal muscle help regulate glucose uptake [8,9], blood flow [10] and contractile force [11].

Recently developed methodologies, especially imaging modalities such as positron emission tomography (PET), provide more information than conventional methodologies to measure regional functions such as hemodynamics and receptor densities in the human body. We have developed several positron-emitting ligands for the purpose of mapping adenosine A_{2A} receptors by PET, and have selected [7-^{11}C]-(*E*)-8-(3,4,5-trimethoxystyryl)-1,3,7-trimethylxanthine ([^{11}C]TMSX) for clinical studies on the brain [12,13]. Further, as a preliminary study, we demonstrated that this radioligand is useful for evaluating cardiac and skeletal muscle by PET [14,15].

Exercise training is known to induce adaptations in several physiological and biochemical functions in both cardiac and skeletal muscle in humans. For cardiac muscle, endurance training induces an increase in contractile function [16] and in resistance to ischemic insult [17]. Adaptations to physical training in skeletal muscle include an increase in capillary density [18], in glucose uptake [19] and in reactive hyperemia [20]. These physiological variables adapted to exercising training seem to be consistent with the known functions mediated by adenosine A_{2A} receptors in these tissues. However, it has not been established whether endurance-trained adaptations have direct effects on these receptors in humans.

In a previous study of [^{11}C]TMSX, using mice, we found that swimming exercise fluctuated the [^{11}C]TMSX-adenosine

* Corresponding author. Tel.: +81 3 3964 3241x3506; fax: +81 3 3964 2188.
E-mail address: ukimura@ieee.org (Y. Kimura).

0969-8051/$ – see front matter © 2005 Elsevier Inc. All rights reserved.
doi:10.1016/j.nucmedbio.2005.07.003

A_{2A} receptor binding in the skeletal muscle [15]. Here we used [^{11}C]TMSX to examine the densities of adenosine A_{2A} receptors in human cardiac and skeletal muscle in young untrained and endurance-trained subjects as the first clinical application to detect physiological changes of adenosine A_{2A} receptors. In our knowledge, any receptor functions in the skeletal muscle of humans and experimental animals have not been evaluated by PET until now.

2. Materials and methods

2.1. Subjects

Five healthy untrained (sedentary) and five endurance-trained subjects (triathlonists) participated in this study (Table 1). The trained subjects were competing at a national college level and trained four to six times per week over 3 years. No subjects had any clinical or laboratory evidence of coronary heart disease, diabetes or systemic hypertension, or were taking any medications. A written informed consent was obtained after the purpose, nature and potential risks of the experiments had been explained to each subject. The Ethics Committee of the Tokyo Metropolitan Institute of Gerontology approved the study protocol.

2.2. Evaluation of adenosine A_{2A} receptors in the cardiac and skeletal muscle by [^{11}C]TMSX and PET

Positron emission tomography scans of [^{11}C]TMSX during a resting state were performed in the thoracic region for each subject as previously described [14,15]. The PET camera used was a SET-2400W model (Shimadzu, Kyoto, Japan), which acquires 63 slices having 128-by-128 voxles each at transverse resolution of 4.5 mm full width of half maximum and at axial resolution of 5.8 mm full width of half maximum. After transmission scanning using a rotating [^{68}Ge]/[^{68}Ga] line source to correct for attenuation, [^{11}C]TMSX was injected intravenously, and dynamic PET scanning was performed for 60 min in two-dimensional mode (10 s×6 frames, 30 s×3 frames, 60 s×5 frames, 150 s×5 frames and 300 s×8 frames). The injected doses of [^{11}C]TMSX were 596±99 MBq and 31±15 nmol. For PET scans, arterial blood was taken at 10, 20, 30, 40, 50, 60, 70, 80, 90, 100, 110, 120, 145, 160, 175 and 180 s, and 5, 7, 10, 15, 20, 30, 40, 50 and 60 min, and the plasma radioactivity was measured. Unaltered [^{11}C]TMSX in the plasma sampled at 3, 10, 20, 30, 40 and 60 min was analyzed by high-performance liquid chromatography [14,15].

Table 1
Physical characteristics of subjects in the untrained and trained groups

	Untrained (n=5)	Trained (n=5)	P
Age (years)	23.4±1.1	21.6±0.9	.24
Height (cm)	170.1±1.8	168.1±2.3	.51
Weight (kg)	64.6±5.3	59.6±3.5	.44
$\dot{V}O_2$ peak (ml kg^{-1} min^{-1})			
Cycling	47.2±3.3	68.8±1.0	.0002
Arm-cranking	32.7±2.1	41.5±2.4	.025

Values are expressed as means±S.E.

Tomographic images were reconstructed using a filtered back-projection method with a cutoff frequency of 1.25 cycle cm^{-1} and a second order filter. The data were collected in a 128×128×31 matrix. The voxel size was 2×2×6.25 mm. Regions of interest (ROIs) were placed on the left ventricular lateral wall, the left ventricular anterior wall, the interventricular septum and the triceps brachii muscle. Time–activity curves (TACs) for the four ROIs and plasma were calculated as Becquerel per milliliter. Using the TACs of tissues and the metabolite-corrected TAC of plasma, we evaluated the total distribution volumes of [^{11}C]TMSX in three regions of the myocardium and triceps brachii muscle using graphical analysis [15,21]; the binding of [^{11}C]TMSX to adenosine A_{2A} receptors was defined as the distribution volume and the ratio of ligand density measured between the blood pool and each tissue in a state of equilibrium. Because anatomical cross-sectional areas of the triceps brachii muscle are greater than elbow flexor muscle groups (i.e., the biceps brachii muscle, the brachialis muscle and the brachioradial muscle) [22], we chose to analyze the triceps brachii muscle.

2.3. Determination of aerobic power peak during cycling and arm-cranking exercises

Maximal aerobic power ($\dot{V}O_2$ peak) was determined using a bicycle ergometer (model 232C50, Combi, Tokyo, Japan), an arm-cranking ergometer (model 881, Monark, Varberg, Sweden) and direct measurement of the rate of oxygen consumption using an automatic gas analyzer (MG360, Minato Medical Science, Tokyo, Japan) and an automatic respiration monitor (RM300, Minato Medical Science) with a continuous incremental protocol.

2.4. Statistical analysis

All data are represented as means±S.E. (n=5 for each group). For physical characteristic parameter, student's unpaired t tests were used to test differences between two groups. For PET parameter, a two-way ANOVA, with groups and muscle as main effects, was used to determine significant differences. If F test was significant, pairwise comparisons were performed by using Scheffe's post hoc test. P<.05 was considered statistically significant.

3. Results

3.1. Peak oxygen uptake

The peak oxygen uptake at both cycling and arm-cranking exercise was significantly higher in the trained subjects than in the untrained subjects (cycling, 68.2±2.2 vs. 47.2±7.4 ml·kg^{-1}·min^{-1}, P<.001; arm-cranking, 41.5±5.4 vs. 32.7±4.7 ml·kg^{-1}·min^{-1}, P<.05; Table 1).

3.2. Typical [^{11}C]TMSX PET images

Fig. 1 shows typical PET images for distribution volume of [^{11}C]TMSX in the chest region of untrained and trained subjects. Some anatomical structures are apparent in the

PET images, and the heart was clearly visualized in both subjects. The myocardium and triceps brachii muscle regions in the trained subjects showed a larger distribution volume compared with those of untrained subjects.

3.3. Differences in distribution volumes of [^{11}C]TMSX between groups

There was no significant difference in the distribution volumes of [^{11}C]TMSX in three regions of myocardium between groups (the interventricular septum, 3.3±0.2 vs. 3.8±0.1 ml g^{-1}; the left ventricular lateral wall, 2.9±0.2 vs. 3.4±0.2 ml g^{-1}; the left ventricular anterior wall, 3.1±0.2 vs. 3.6±0.1 ml g^{-1}, untrained vs. trained subjects, respectively). To eliminate the possible error of PET signals due to the spatial resolution in the restricted area of the myocardium, the distribution volume of [^{11}C]TMSX in the whole myocardium was also evaluated and compared with that in triceps brachii muscle (Fig. 2). In both groups, the distribution volume in the whole myocardium was significantly (P<.0001) greater than that in the triceps brachii muscle. Further, in the cardiac and the triceps brachii muscle, distribution volumes of [^{11}C]TMSX in the trained subjects were significantly (P<.001) greater than those in untrained subjects.

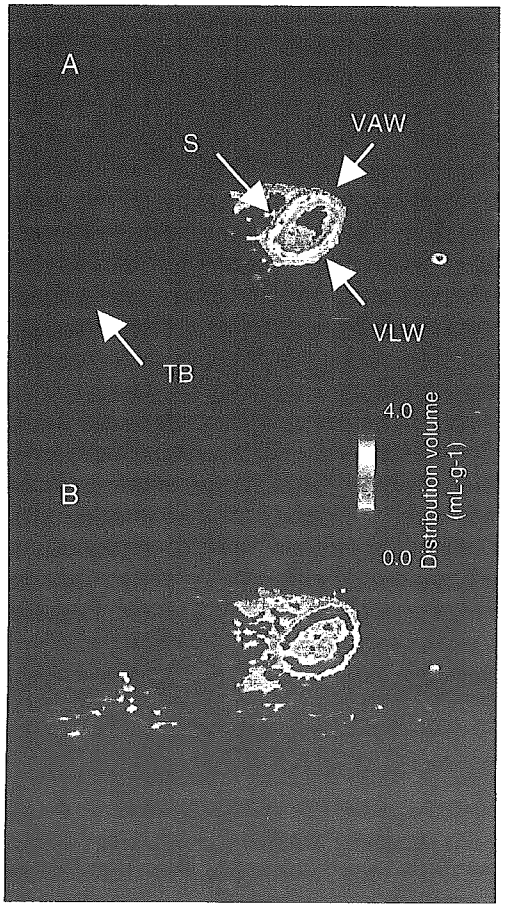

Fig. 1. Typical PET images of the distribution volume of [^{11}C]TMSX in the thoracic region of untrained and trained subjects. (A) Untrained subject. (B) Trained subject. VLW, left ventricular lateral wall; VAW, left ventricular anterior wall; S, inter ventricular septum; TB, triceps brachii muscle.

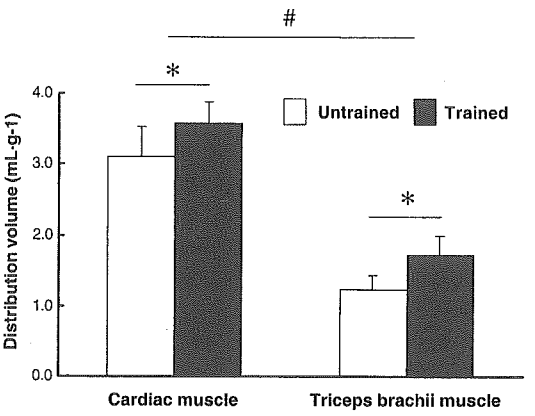

Fig. 2. Distribution volumes of [^{11}C]TMSX in the cardiac and triceps brachii muscles of untrained and trained subjects. The value for the cardiac muscle is calculated as a mean distribution volume for the three regions studied (i.e., left ventricular lateral wall, left ventricular anterior wall, and inter ventricular septum). Open bar, untrained group; solid bar, trained group. *Significant difference, untrained subjects < trained subjects (P<.001). #Significant difference, cardiac muscle > triceps brachii muscle (P<.0001) in each group.

4. Discussion

We applied [^{11}C]TMSX PET to the detection of physiological changes in adenosine A_{2A} receptors in cardiac and skeletal muscle induced by physical training. We found that cardiac muscle has a greater density of adenosine A_{2A} receptors than skeletal muscle, and that endurance-trained subjects have the greater adenosine A_{2A} receptor densities in cardiac and skeletal muscle compared with untrained subjects.

4.1. Differences in distribution volume of [^{11}C]TMSX between cardiac and triceps brachii muscles

Dixon et al. [23] reported that, in rats, adenosine A_{2A} receptor mRNA is widely distributed in peripheral organs such as the lung, eye and skeletal muscle, whereas adenosine A_1 receptors are located in the central nervous system and heart. We found here that the distribution volume in muscle was 44% of that of the myocardium in the present study. Thus, the human myocardium has a greater density of adenosine A_{2A} receptors than skeletal muscle.

4.2. Effects of endurance training on adenosine A_{2A} receptor in the cardiac muscle

Although there was not a statistically significant difference between endurance-trained and untrained subjects for the individual myocardial ROIs, there was a clear trend for the distribution volumes of [^{11}C]TMSX to be greater in the trained subjects than in the untrained subjects (see Results). When evaluating the whole myocardium to eliminate the possible error of PET signals due to the spatial resolution in the restricted area, the distribution volumes of

[^{11}C]TMSX in the myocardium were significantly greater in the trained subjects than in the untrained subjects (Fig. 2). Endurance training induces an increase in contractile function [12] and in resistance to ischemic insult [13] in myocardium. Adenosine A_{2A} receptor in the myocardium may involve an acquisition of the resistance to ischemia [4,5] and may modulate contraction [6,7]. Thus, our results suggest that greater adenosine A_{2A} receptors induced by chronic endurance training in the myocardium might contribute to myocardial tolerance to ischemia and contractile function in the myocardium.

Coronary blood flow distribution is different between epicardium and endocardium: blood flow is higher in endocardium than in epicardium [24]. Furthermore, regional differences between endocardium and epicardium were found not only in effects of exercising training on contractile and biochemical properties [25] but also in coronary arteriolar dilation to adenosine [26]. However, PET cannot distinguish between endocardium blood flow and epicardium blood flow because of spatial resolution of the PET camera. Kalliokoski et al. [27] found no significant differences in the myocardial blood flow of the interventricular septum, the left ventricular lateral wall and the left ventricular anterior wall between untrained and endurance-trained subjects both at resting and adenosine-stimulated myocardium, where endocardium and epicardium were included. Extrapolating basal myocardial perfusion reported by Kalliokoski et al. [27], no relationship was found between the distribution volume of the [^{11}C]TMSX in the present study and the regional myocardial perfusion in their study (r=.006, P=.99). Therefore, it is unlikely that the difference of the distribution volume of the [^{11}C]TMSX between untrained and trained subjects related to distribution of myocardial perfusion, although myocardial blood flow was not measured in the present study. It is noticed that the changes of blood flow is included in the quantitative evaluation of the distribution volume of the [^{11}C]TMSX in the myocardium.

In contrast, using blood flow data during adenosine-stimulated hyperemia [27], however, produced a greater correlation coefficient but did not reach statistical significance (r=.603, P=.23); a greater densities of adenosine A_{2A} receptors induces a higher blood flow during adenosine-stimulated hyperemia. These suggest that effect of physical training is not visible at resting but at stimulating state.

4.3. Effects of endurance training on adenosine A_{2A} receptors in the triceps brachii muscle

The distribution volume of [^{11}C]TMSX in the myocardium and triceps brachii muscle of the trained group was significantly greater than that of the untrained group (Fig. 2). This indicates an increase in the adenosine A_{2A} receptor density. Lynge and Hellsten [28] showed, using immunohistochemistry, that in humans, the adenosine A_{2A} and A_{2B}, but not the A_1, receptors were present in the plasma membrane and cytosol of skeletal muscle, whereas all three subtypes, A_1, A_{2A} and A_{2B}, were in vascular smooth muscle and endothelial cells. They also found that the cytosolic staining of the adenosine A_{2A} receptors was slightly more intense in type I muscle fibers, whereas the A_1 receptor was almost absent [28]. As the peak oxygen uptake during the arm-cranking exercise, defined as aerobic capacity in upper body, was significantly higher in the trained subjects than in the untrained subjects (Table 1), the higher adenosine A_{2A} receptor density found here could be explained by differences in capillary density [18] or percentage of type I fibers in the triceps brachii muscle [28]. As discussed above, the spatial resolution of PET cannot discriminate the endothelial cells from muscle. Haas et al. [18] indicated a 25% increase in capillary density induced by chronic muscle stimulation, which apparently corresponds to an increase in the distribution volume of [^{11}C]TMSX in the present study. However, it is unlikely that the PET parameter adequately reflects information of endothelial cells in resting muscle because the capillary in skeletal muscle is not open at resting state [29]. Actually, there are no significant differences in the skeletal muscle blood flow and blood volume evaluated with PET between untrained and trained subjects at rest [30]. Thus, the contribution of endothelial cells may be minor in a greater distribution volume of [^{11}C]TMSX in the endurance-trained muscle at least in resting state, although we could not completely exclude the possibility that greater distribution volume of [^{11}C]TMSX reflects increased capillary density with endurance training.

It has been well documented that training effects for muscle functions are more pronounced during exercise compared with at rest, as demonstrated by Kalliokoski et al. [30]. Exercise training increases physiological functions mediated by adenosine A_{2A} receptors such as capillary density (26~36%) [18], glucose uptake (34%) [19] and reactive hyperemia (35%) [20]. In the present study, 42% increases in the distribution volume of the [^{11}C]TMSX in the skeletal muscle could be found in the trained subjects, whereas only 16% increases in the cardiac muscle. Further investigations, such as [^{11}C]TMSX PET measurements during exercise and/or under exogenously maximal vasodilation, are needed to clarify responsible mechanism(s) for a larger density of adenosine receptors in skeletal muscle.

4.4. Validity of evaluating for adenosine A_{2A} receptors with [^{11}C]TMSX and PET

We have proposed using [^{11}C]TMSX as a radioligand for mapping adenosine A_{2A} receptors in the brain [12,13], heart [14] and skeletal muscle [15] by PET. The specific binding of [^{11}C]TMSX to adenosine A_{2A} receptors in skeletal muscle has been validated in animal and human studies [15]. As a feasibility study for detecting possible changes in the ligand-receptor binding, in mice undertaking forced swimming, we found lower uptake of [^{11}C]TMSX in the cardiac and skeletal muscle. The finding could be explained by an endogenous adenosine levels by exercise, which resulted in inhibition

of [^{11}C]TMSX-adenosine A_{2A} receptors binding [15]. In humans, a blocking study using theophylline, a nonselective adenosine A_{2A} receptor antagonist used clinically as an antiasthmatic, clearly demonstrated specific binding of [^{11}C]TMSX to the adenosine A_{2A} receptors in the cardiac and skeletal muscle [15]. Thus, this technique is expected to be able to detect biological changes in the density of adenosine A_{2A} receptors and/or ligand-receptor binding associated with changes in endogenous adenosine concentrations. In the present study, we performed [^{11}C]TMSX PET in two independent groups with and without endurance training; however, PET evaluation before and after the task such as exercise is also of great interest.

4.5. [^{11}C]TMSX PET for cardiac and skeletal muscle physiology

Positron emission tomography has been used for cardiac and skeletal muscle physiology from the 1990s, especially in the Turku PET center in Finland [31,32]. It has a great advantage over conventional methodology to measure regional physiological functions in vivo and provides many significant findings. We have reported regional differences in hemodynamics in resting [33] and recovered muscle [34]. However, this was the first use of this approach to evaluate the impact of training on cardiac and muscle physiology.

Physiological variables adapted to exercising training seem to be consistent with the known functions mediated by adenosine A_{2A} receptors in cardiac and skeletal muscle. However, it has not been established whether endurance-trained adaptations have direct effects on these receptors in humans. As an initial approach, to address this question, we used a cross-sectional study design in this investigation. Because of the limitations associated with this design, we attempted to isolate the influence of endurance training as much as possible. To do so, untrained and endurance-trained subjects were carefully matched for age, height and weight (Table 1). Our present results indicate that chronic endurance training is associated with greater densities of adenosine A_{2A} receptor in endurance-trained subjects. Nevertheless, these results of the present cross-sectional study needs to be confirmed with the exercise intervention study in the future.

In conclusion, the distribution volumes of [^{11}C]TMSX in the cardiac and skeletal muscles of the endurance-trained group were significantly greater than those of the untrained group. These results suggest that endurance training increases the densities of adenosine A_{2A} receptors in both the cardiac and skeletal muscles in young humans. [^{11}C]TMSX PET has potential for use in studies on adenosine A_{2A} receptors in both cardiac and skeletal muscle physiology.

Acknowledgments

This work was supported by grant-in-aid for scientific research (B) no. 16390348 from the Japan Society for the promotion of Science. We thank Dr. Kazunori Kawamura for manufacture of the radiopharmaceuticals and Ms. Miyoko Ando for care of the subjects during the PET measurements.

References

[1] Dunwiddie TV, Masino SA. The role and regulation of adenosine in the central nervous system. Annu Rev Neurosci 2001;24:31–55.
[2] Shryock JC, Belardinelli L. Adenosine and adenosine receptors in the cardiovascular system: biochemistry, physiology, and pharmacology. Am J Cardiol 1997;79:2–10.
[3] Olah ME, Stiles GL. Adenosine receptor subtypes: characterization and therapeutic regulation. Annu Rev Pharmacol Toxicol 1995;35: 581–606.
[4] Lozza G, Conti A, Ongini E, Monopoli A. Cardioprotective effects of adenosine A_1 and A_{2A} receptor agonists in the isolated rat heart. Pharmacol Res 1997;35:57–64.
[5] Shryock JC, Snowdy S, Baraldi PG, Cacciari B, Spalluto G, Monopoli A, et al. A_{2A}-adenosine receptor reserve for coronary vasodilation. Circulation 1998;98:711–8.
[6] Dobson JG, Fenton RA. Adenosine A_2 receptor function in rat ventricular myocytes. Cardiovasc Res 1997;34:337–47.
[7] Monahan TS, Sawmiller DR, Fenton RA, Dobson Jr JG. Adenosine A_{2a}-receptor activation increases contractility in isolated perfused hearts. Am J Physiol 2000;279:H1472–81.
[8] Derave W, Hespel P. Role of adenosine in regulating glucose uptake during contractions and hypoxia in rat skeletal muscle. J Physiol 1999; 515:255–63.
[9] Han DH, Hansen PA, Nolte LA, Holloszy JO. Removal of adenosine decreases the responsiveness of muscle glucose transport to insulin and contractions. Diabetes 1998;47:1671–5.
[10] Poucher SM. The role of the A_{2A} adenosine receptor subtype in functional hyperaemia in the hindlimb of anaesthetised cats. J Physiol 1996;492:495–503.
[11] Clark KI, Barry SR. Aminophylline enhances resting Ca^{2+} concentrations and twitch tension by adenosine receptor blockade in *Rana pipiens*. J Physiol 1994;481:129–37.
[12] Ishiwata K, Wang WF, Kimura Y, Kawamura K, Ishii K. Preclinical studies on [^{11}C]TMSX for mapping adenosine A_{2A} receptors by positron emission tomography. Ann Nucl Med 2003;17:205–11.
[13] Ishiwata K, Mishina M, Kimura Y, Oda K, Sasaki T, Ishii K. First visualization of adenosine A_{2A} receptors in the human brain by positron emission tomography with [^{11}C]TMSX. Synapse 2004;55: 133–6.
[14] Ishiwata K, Kawamura K, Kimura Y, Oda K, Ishii K. Potential of an adenosine A_{2A} receptor antagonist [^{11}C]TMSX for myocardial imaging by positron emission tomography: a first human study. Ann Nucl Med 2003;17:457–62.
[15] Ishiwata K, Mizuno M, Kimura Y, Kawamura K, Oda K, Sasaki T, et al. Potential of [^{11}C]TMSX for evaluation of adenosine A_{2A} receptors in the skeletal muscle by positron emission tomography. Nucl Med Biol 2004;31:949–56.
[16] Tibbits GF, Barnard RJ, Baldwin KM, Cugalj N, Roberts NK. Influence of exercise on excitation–contraction coupling in rat myocardium. Am J Physiol 1981;240:H472–80.
[17] Brown DA, Jew KN, Sparagna GC, Musch TI, Moore RL. Exercise training preserves coronary flow and reduces infarct size after ischemia-reperfusion in rat heart. J Appl Physiol 2003;95:2510–8.
[18] Haas TL, Milkiewicz M, Davis SJ, Zhou AL, Egginton S, Brown MD, et al. Matrix metalloproteinase activity is required for activity-induced angiogenesis in rat skeletal muscle. Am J Physiol 2000;279: H1540–7.
[19] Fujimoto T, Kemppainen J, Kalliokoski KK, Nuutila P, Ito M, Knuuti J. Skeletal muscle glucose uptake response to exercise in trained and untrained men. Med Sci Sports Exerc 2003;35:777–83.